The Astronomical Journal, 152:114 (20pp), 2016 November doi:10.3847/0004-6256/152/5/114

ROTATION IN THE PLEIADES WITH *K2*. II. MULTIPERIOD STARS

L. M. Rebull[1,2], J. R. Stauffer[2], J. Bouvier[3], A. M. Cody[4], L. A. Hillenbrand[5], D. R. Soderblom[6,7], J. Valenti[6,7], D. Barrado[8], H. Bouy[8], D. Ciardi[9], M. Pinsonneault[10,11], K. Stassun[12,13], G. Micela[14], S. Aigrain[15], F. Vrba[16], G. Somers[10,11], E. Gillen[15,17], and A. Collier Cameron[18]

[1] Infrared Science Archive (IRSA), Infrared Processing and Analysis Center (IPAC), 1200 E. California Boulevard, California Institute of Technology, Pasadena, CA 91125, USA; rebull@ipac.caltech.edu
[2] Spitzer Science Center (SSC), Infrared Processing and Analysis Center (IPAC), 1200 E. California Boulevard, California Institute of Technology, Pasadena, CA 9112, USA
[3] Université de Grenoble, Institut de Planétologie et d'Astrophysique de Grenoble (IPAG), F-38000 Grenoble, France; CNRS, IPAG, F-38000 Grenoble, France
[4] NASA Ames Research Center, *Kepler* Science Office, Mountain View, CA 94035, USA
[5] Astronomy Department, California Institute of Technology, Pasadena, CA 91125, USA
[6] Space Telescope Science Institute, 3700 San Martin Drive, Baltimore, MD 21218, USA
[7] Center for Astrophysical Sciences, Johns Hopkins University, 3400 North Charles Street, Baltimore, MD 21218, USA
[8] Centro de Astrobiología, Dpto. de Astrofísica, INTA-CSIC, E-28692, ESAC Campus, Villanueva de la Cañada, Madrid, Spain
[9] NASA Exoplanet Science Institute (NExScI), Infrared Processing and Analysis Center (IPAC), 1200 E. California Boulevard, California Institute of Technology, Pasadena, CA 91125, USA
[10] Department of Astronomy, The Ohio State University, Columbus, OH 43210, USA
[11] Center for Cosmology and Astroparticle Physics, The Ohio State University, Columbus, OH 43210, USA
[12] Department of Physics and Astronomy, Vanderbilt University, Nashville, TN 37235, USA
[13] Department of Physics, Fisk University, Nashville, TN 37208, USA
[14] INAF—Osservatorio Astronomico di Palermo, Piazza del Parlamento 1, I-90134, Palermo, Italy
[15] Department of Physics, University of Oxford, Keble Road, Oxford OX3 9UU, UK
[16] US Naval Observatory, Flagstaff Station, P.O. Box 1149, Flagstaff, AZ 86002, USA
[17] Astrophysics Group, Cavendish Laboratory, J.J. Thomson Avenue, Cambridge CB3 0HE, UK
[18] School of Physics and Astronomy, University of St. Andrews, North Haugh, St. Andrews, Fife KY16 9SS, UK

Received 2016 April 29; revised 2016 May 31; accepted 2016 May 31; published 2016 October 11

ABSTRACT

We use *K*2 to continue the exploration of the distribution of rotation periods in Pleiades that we began in Paper I. We have discovered complicated multiperiod behavior in Pleiades stars using these *K*2 data, and we have grouped them into categories, which are the focal part of this paper. About 24% of the sample has multiple, real frequencies in the periodogram, sometimes manifesting as obvious beating in the LCs. Those having complex and/or structured periodogram peaks, unresolved multiple periods, and resolved close multiple periods are likely due to spot/spot group evolution and/or latitudinal differential rotation; these largely compose the slowly rotating sequence in P versus $(V-K_s)_0$ identified in Paper I. The fast sequence in P versus $(V-K_s)_0$ is dominated by single-period stars; these are likely to be rotating as solid bodies. Paper III continues the discussion, speculating about the origin and evolution of the period distribution in the Pleiades.

Key words: galaxies: clusters: individual (Pleiades) – stars: rotation

Supporting material: machine-readable table

1. INTRODUCTION

Ultrahigh-precision photometry can reveal a wealth of multifrequency behavior, and indeed, one of the original goals of the *Kepler* mission was to investigate asteroseismology (e.g., Metcalfe et al. 2009) and stellar cycles, including differential rotation (e.g., Karoff et al. 2009). Rotation rates and timescales for stellar cycles are thought to be a function of age of the star. The original *Kepler* field, however, had no clusters younger than 1 Gyr. With the repurposed *K*2 mission (Howell et al. 2014) comes the opportunity to study clusters of a much wider range of ages, with the potential to constrain measures of, say, surface differential rotation at much younger ages.

The Pleiades is populous (over 1000 members; e.g., Bouy et al. 2015), relatively young (125 Myr; Stauffer et al. 1998), and nearby (136 pc; Melis et al. 2014). As such, it provides a nearly ideal laboratory for studying rotation of young stars, including surface differential rotation and spot or spot group evolution. These stars are old enough to have completed all of their pre-main-sequence accretion and most of their pre-main-sequence contraction, but they are still young enough to be rotating quickly enough that there are at least six to seven complete rotations over a *K*2 campaign (~70 days long), and their spots/spot groups are large enough to produce brightness variations easily detectable by *K*2 ($\gtrsim$0.003 mag).

Rebull et al. (2016, hereafter Paper I) presented the *K*2 Pleiades data and reduction, membership selection, and our general results. About 92% of the members in our sample have at least one measured spot-modulated rotation period. The overall relationship between P and $(V-K_s)_0$ follows the overall trends found in other Pleiades studies (e.g., Hartman et al. 2010; Covey et al. 2016). There is a slowly rotating sequence for $1.1 \lesssim (V-K_s)_0 \lesssim 3.7$ (2 days $\lesssim P \lesssim$ 11 days) and a primarily rapidly rotating population for $(V-K_s)_0 \gtrsim 5.0$ (0.1 days $\lesssim P \lesssim$ 2 days). There is a region in which there seems to be a disorganized relationship between P and $(V-K_s)_0$ for $3.7 \lesssim (V-K_s)_0 \lesssim 5.0$ (0.2 days $\lesssim P \lesssim$ 15 days).

In the analysis conducted as part of Paper I, we noticed that a significant fraction of the periodograms, ~30%, had additional, significant peaks in the periodogram. In these cases, the false-alarm probability (FAP) for the additional peaks was just as

low as that for the main peak, often calculated to be exactly 0. The *K*2 light curves (LCs) are so exquisite that when subsidiary peaks appear as significant, it is worth investigating, which is the motivation for this paper.

In this paper, we focus on the diversity of multifrequency periodograms and LCs we find in these *K*2 Pleiades data. Section 2 summarizes the key points of the observations and data reduction from Paper I. Section 3 describes the several categories of LCs and periodogram structures that we found in the *K*2 data. The simplest division of the LCs and periodograms is into single- and multiperiod stars; the distributions of these broad categories are discussed in Section 4. However, we have many more than just two categories of LCs and periodogram structures; Section 5 looks at where these various categories of objects fall. Section 6 looks at the distribution of period differences. Section 7 summarizes our main results. This is the second of three papers focused on rotation periods in the Pleiades. Stauffer et al. (2016, hereafter Paper III) continues the discussion of these Pleiades results, focusing on the physical origins of the *P* distribution.

2. OBSERVATIONS AND METHODS

The observations and methods are discussed in detail in Paper I. Here we simply summarize the main points:

1. Members of the Pleiades were observed in *K*2 campaign 4, which lasted for 72 days. All of the stars in this sample were observed in the long-cadence (~30 minute exposure) mode.
2. We looked for periods using the Lomb–Scargle (LS; Scargle 1982) approach.
3. For stars of the mass range considered here, the periods that we measure are, by and large, starspot-modulated rotation periods. Spot modulation is the simplest explanation for sinusoidal (or sinusoidal-like) variations where there are changes over an entire orbital phase.
4. We assembled a catalog of literature data for our targets. The most important values obtained from this search are $(V - K_s)_0$ (measured or inferred; see Paper I) and membership (see Paper I). Table 1 includes the most relevant supporting data from Paper I. Cross-IDs between the EPIC number, R.A./decl., and common literature names are in Paper I.
5. Out of the 1020 LCs of candidate Pleiades members from which we started, there are 775 high-confidence members, with 51 more lower-confidence members (for a total of 826 members). Table 1 includes these numbers.
6. Out of those 775 (best members), 716 (92.4%) have at least one measured period that we believe in the overwhelming majority of cases to be a rotation period and due to starspots. Including the lower-confidence members, 759/826 (91.9%) have at least one measured period.
7. The period distribution is strongly peaked at $P < 1$ day with typical amplitudes of ~0.03 mag.

Table 2 includes the LC categories for each star as introduced in this paper.

As stated above, what drove us to investigate the multiperiod behavior was the presence of additional, significant (low FAP) peaks in the periodogram. To first order, we took the periods in order of peak strength (and thus significance); all other things being equal, the highest peak is what we took to be the primary period, P_1, the second highest peak is what we took to be the secondary peak, P_2, etc. However, in some cases, we had to overrule that ordering of the periods (see, e.g., Section 3.1).

3. EMPIRICAL STRUCTURES IN THE LCS AND POWER SPECTRA

While inspecting the power spectra of the ensemble of *K*2 LCs, about 60% of the ensemble had properties as found in Figure 2 of Paper I, where there was just one sinusoidal periodic signal, and it was unambiguously periodic (very low FAP), with just one period. However, we noted that about 30% of the sample potentially had more than one significant period in the power spectrum, where the FAP was just as low for these additional peaks. We phased the LCs at these additional peaks, and in many cases, the phased LC is just as convincing as the LC phased at the main peak.

We noticed patterns in the power spectra (and/or the original and phased LCs), which enabled us to group these multiperiod objects into categories, which we discuss in this section, and summarize in Table 1. Note that objects can simultaneously belong to more than one of these categories. We conclude this section by discussing the ensemble incidence rate of multiperiod LCs. For all of the discussion here, "the sample" denotes members of the right brightness range, as described in Paper I and Table 1.

For those stars where we can distinguish multiple plausible frequencies, we have included in Table 2 the secondary (and tertiary or even quaternary in some cases) periods. The first period that is listed is the strongest period and/or the one we believe to be the rotation rate of the star. Some of these stars are known or inferred binaries; in these cases, the period should most often be that of the primary. If they are unresolved multiples, we cannot assign directly measured K_s or $(V - K_s)_0$ to the companion, so these companions do not appear as separate stars in our analysis (here or in Paper I or Paper III).

Finally, for completeness, we note that in a few cases it was difficult to determine whether a subsidiary peak in the peridogram was a harmonic (usually half the true *P*) or an independent period. Our primary discriminent was by eye—if the LC phased to a subsidiary peak had characteristics of a harmonic (e.g., a wide distribution of fluxes at most phases and a "criss-cross" appearance of the phased LC), then we took it to be a harmonic and did not include it as an independent period derived from our data. For most of these cases where the by-eye assessment identified the subsidiary peak as a harmonic, the ratio of the true *P* to the harmonic was very close to 2. Based on that, even if the phased LC did not obviously appear to be a harmonic, but the ratio of the periods was within 3% of 2 ($1.97 < P_1/P_2 < 2.03$), then we took the periods to be, in fact, harmonics, and did not retain the shorter *P* as an independent, second period.

3.1. Double-dipped LCs

For sinsusoidal, single-period LCs, as seen in Figure 2 of Paper I, if there is a secondary peak in the power spectrum, it is very weak relative to the main peak. However, many of the LCs have double-dipped (or double-humped) structure in their phased LCs.[19] When the two dips are of comparable depth and fraction of the orbital phase, there is enough power in the $P/2$ harmonic that it appears with comparable strength in the periodogram. Taken at face value, then, such a power spectrum makes the star appear to have (at least) two significant periods; see Figure 1. Sometimes the $P/2$ peak is of comparable strength to the *P* peak, and sometimes the $P/2$ harmonic is actually the dominant peak (perhaps by a considerable margin)

[19] McQuillen et al. (2013) use this same terminology for similar LCs.

Table 1
Star/Light-curve/Periodogram Categories[a]

Name	Number	Frac. of Sample[b]	Frac. of Periodic Sample[c]	Empirical Properties	Possible Physical Interpretation
Initial sample (see Paper I)	1020	…	…	All *K*2 LCs of candidate Pleiades members	…
Best members (see Paper I)	775	…	…	Highest-confidence (our determination) Pleiades members with *K*2 LCs, and neither too bright nor too faint ($6 < K_s < 14.5$)	…
OK members (see Paper I)	51	…	…	Lower-confidence (our determination) Pleiades members with *K*2 LCs, and neither too bright nor too faint ($6 < K_s < 14.5$)	…
The sample, aka the sample of members	826	1.00	…	The set of all high-confidence ("best") plus lower-confidence ("ok") members that are neither too bright nor too faint ($6 < K_s < 14.5$)	…
The periodic sample	759	0.92	1.00	The subset of all high-confidence ("best") plus lower-confidence ("ok") members that are neither too bright nor too faint ($6 < K_s < 14.5$) and are found to be periodic by us in these *K*2 data	…
Single frequency	559	0.68	0.74	The star has just one detectable period. Could be sinusoid or other shapes, but there is just one detectable period.	Single spot/spot group rotating into and out of view
Double-dipped (or double-humped)	107	0.13	0.14	There is a double-dipped (or double-humped) structure in the phased LC, *and* the power spectrum has a substantial amount of power in the harmonic ($P/2$) compared to the main *P*.	Two spot/spot groups, well separated in longitude, rotating into and out of view
Moving double-dip	31	0.038	0.041	*(Effectively a subcategory of both double-dip and shape changers.)* There is a double-dipped (or double-humped) structure in the phased LC, *and* often the power spectrum has a substantial amount of power in the harmonic ($P/2$) compared to the main *P*, *and* one can see by eye that one structure in the LC is moving with respect to the other structure over the campaign.	Spot/spot group evolution and/or latitudinal differential rotation
Shape changer	114	0.14	0.15	Shape of the LC changes over the campaign, but not enough such that a separate period can be derived. Usually, these are single-period stars.	Latitudinal differential rotation and/or spot/spot group evolution
Orbiting clouds?	5	0.0061	0.0066	The phased LCs show shallow, angular dips that cover a relatively small portion of the total phase. (NB: one more is formally an NM, for a total of 6)	Orbiting clouds or debris??
Multifrequency	200	0.24	0.26	More than one frequency is measured, or apparent by eye (in the periodogram or the LC itself) even if specific value cannot be determined.	Spot/spot group evolution and/or latitudinal differential rotation and/or binarity
Beater	135	0.16	0.18	Light curve appears to have beating signatures by eye (e.g., changing envelope over the campaign).	Spot/spot group evolution and/or latitudinal differential rotation
Complex peak	89	0.11	0.12	Peak in power spectrum is structured (multicomponent) or wider than expected for that period.	Latitudinal differential rotation and/or spot/spot group evolution
Resolved multiperiod, close	126	0.15	0.17	Well-resolved, very narrow peaks in the power spectrum and both periods are real. The periods are very close together by the $\Delta P/P$ metric.	Latitudinal differential rotation and/or spot/spot group evolution in most cases; binarity in other cases
Resolved multiperiod, distant	37	0.045	0.049	Well-resolved, very narrow peaks in the power spectrum and both periods are real. The periods are *NOT* very close together by the $\Delta P/P$ metric.	Binarity
Pulsator	8	0.0097	0.011	"Forest" of short-period peaks in the periodogram.	Pulsation (δ Scuti)

Notes.
[a] The first half of this table includes numbers discussed in detail in Paper I. The second half of this table is a high-level summary of the categories discussed in detail in Section 3. Please see the text for a much longer discussion of properties and interpretation.
[b] Fraction out of "the sample," e.g., 826. Stars can belong to more than one category, so the fractions do not add to 1.
[c] Fraction out of "the periodic sample," e.g., 759. Stars can belong to more than one category, so the fractions do not add to 1.

Table 2
Periods, Supporting Data, and Light-curve Categories for Periodic Pleiades

Label	Contents
EPIC	Number in the Ecliptic Plane Input Catalog (EPIC) for *K*2
IAU	IAU identifier
coord	R.A. and decl. (J2000) for target
Alias	Other identifier
Vmag	V magnitude (in Vega mag), if observed
Kmag	K_s magnitude (in Vega mag), if observed
vmk0	$(V-K_s)_0$—dereddened $V-K_s$, directly observed (if V and K_s exist) or inferred (see text)
P1	Primary period, in days (taken to be rotation period)
P2	Secondary period, in days
P3	Tertiary period, in days
P4	Quaternary period, in days
ampl	Amplitude, in mag, of the 10th to the 90th percentile
memb	Membership indicator: Best, OK, or NM
single/multi-P	Indicator of whether single or multiperiod star
dd	Indicator of whether or not it is a double-dip LC
ddmoving	Indicator of whether or not it is a moving double-dip LC
shch	Indicator of whether or not it is a shape changer
beat	Indicator of whether or not the full LC has beating visible
cpeak	Indicator of whether or not the power spectrum has a complex, structured peak and/or has a wide peak
resclose	Indicator of whether or not there are resolved close periods in the power spectrum
resdist	Indicator of whether or not there are resolved distant periods in the power spectrum
pulsator	Indicator of whether or not the power spectrum and period suggest that this is a δ Scuti pulsator
cloud	Indicator of whether or not the phased LC has narrow, angular dips

(This table is available in its entirety in machine-readable form.)

in the periodogram. (Recall that the LS approach is fitting sinusoids, so the relative strength of the peaks is related to the strength of the single sinusoidal nature of the periodicity.) For these cases, visual inspection reveals that the true rotation period is actually P and not $P/2$, as shown in Figure 1. The peaks are typically very narrow, suggesting a limited range of frequencies found around the period (and $P/2$) during the campaign. About 14% of the sample (and 15% of the periodic sample) has this kind of power spectrum and phased LC shape.

We identified the double-dip LC types by eye, but we considered both the properties of the phased LC shape and the structures of the periodogram. To be in the double-dip category, there has to be double-dip (or double-hump) structures in the phased LC, as well as substantial power in the nominally subsidiary peak $P_{\rm true}/2$. (In other words, the periodogram has to look like it has two significant periods, but in reality only one of the pair is a viable period.)[20] Therefore, we do not include in this category those LCs that have multiple dips/humps in the phased LC where the ratio of the peak power values for the correct P and the first subsidiary peak is large. A phased LC with two (or more) dips of very different shape or relative duration will result in the power spectrum correctly identifying the right period, with little power in the harmonics. (For examples of LCs where there are multiple dips but nearly all the power is in the correct P, see the single-period examples in Figure 6 below.) For all the single-period, ∼sinusoidal LCs in our set, the median ratio of the power of the main peak (in the periodogram) to the second peak power is ∼14. For the double-dip LCs, the median of this power ratio is ∼2.

In some cases, inspection of the LC shows a double-dip structure over only part of the *K*2 campaign, or there are other slow changes over the *K*2 campaign such that the double-dip structure may be transient or the location of one of the minima changes slowly with respect to the maxima over the campaign. These changes are not large enough to, on their own, generate enough power in a secondary period, so no secondary period can be identified; these changes also mean that the power may not be redistributed into a subsidiary peak to the same degree as the rest of this category for a periodogram calculated over the entire *K*2 campaign. These so-called "moving double-dip" stars are identified by eye and are a subcategory of the overall double-dip category; examples are given in Figure 2. (These moving double-dip stars are also "shape changers"; see Section 3.5.)

Most of the stars in this category have only one real period. However, some of these double-dip LCs have at least one additional periodic signal, which may or may not also have the same double-dip effect that rearranges the power distribution. (For an example where two periods are found that are both double-dip, see 211054634/HHJ291 in Figure 4 below.)

For completeness, we add that there are a few borderline cases (such as 211048126/HII 1321) where the power spectrum has some signatures of this sort of effect (harmonic at 2P rather than $P/2$, and/or strong harmonic at $P/2$), but the phased LC is not convincing. Those have not been included in this category.

These double-dip LC structures are most likely to be caused by spots well separated in longitude on the star, as in Davenport et al. (2015). The Fourier transform of the LC of a low-latitude spot viewed equator-on on a limb-darkened star has significant power in its first harmonic because there is a flat plateau when the spot is behind the star. The resulting LC is well approximated by a combination of the fundamental and its first harmonic. For this reason, starspot distributions of arbitrary complexity always give either single-humped or double-humped LCs, the exact morphology depending on the degree of departure from axisymmetry. If there are two concentrations of spots on opposite hemispheres, the fundamental cancels but the first harmonics from both groups reinforce each other, giving an apparently stronger signal in the first harmonic. (Also see Russell 1906 for a discussion of similar phenomena in the context of asteroid shapes.)

There is no preferential $(V-K_s)_0$ color for double-dip objects on the whole (see discussion in Section 5); they are found at all colors for which we have *K*2 spot-modulated LCs, as would be expected for spot periods. However, there are strong correlations between the stability of the pattern and $(V-K_s)_0$; the moving double-dip objects are all earlier types, with $1 \lesssim (V-K_s)_0 \lesssim 4.6$ (FGK and early M). Almost all the stationary double-dip objects have $(V-K_s)_0 \gtrsim 4$; there are a few with $3 \lesssim (V-K_s)_0 \lesssim 4$.

[20] This feature, where the periodogram looks like it has two significant periods but in reality has only one real period, accounts for the apparent discrepancies in some of the sample fractions given. At the end of the analysis: (a) 59% have one and only one period and a ∼sinusoidal LC. (b) 68% have one and only one period, consisting of both the ∼sinusoidal LC and those double-dip LCs that look like they have two significant periods but in reality have only one. (c) When approaching the analysis of the LCs with *potentially* more than one significant peak in the periodogram, therefore, we include all the stars that in the end legitimately have more than one period, plus the double-dip stars that only appear to have more than one period (noting that some double-dip stars do legitimately have more than one real period). Therefore, 33% of the sample has *potentially* more than one significant peak in the periodogram, which then decreases to 24% actually having multiple frequencies in the end. (8% are not periodic at all.)

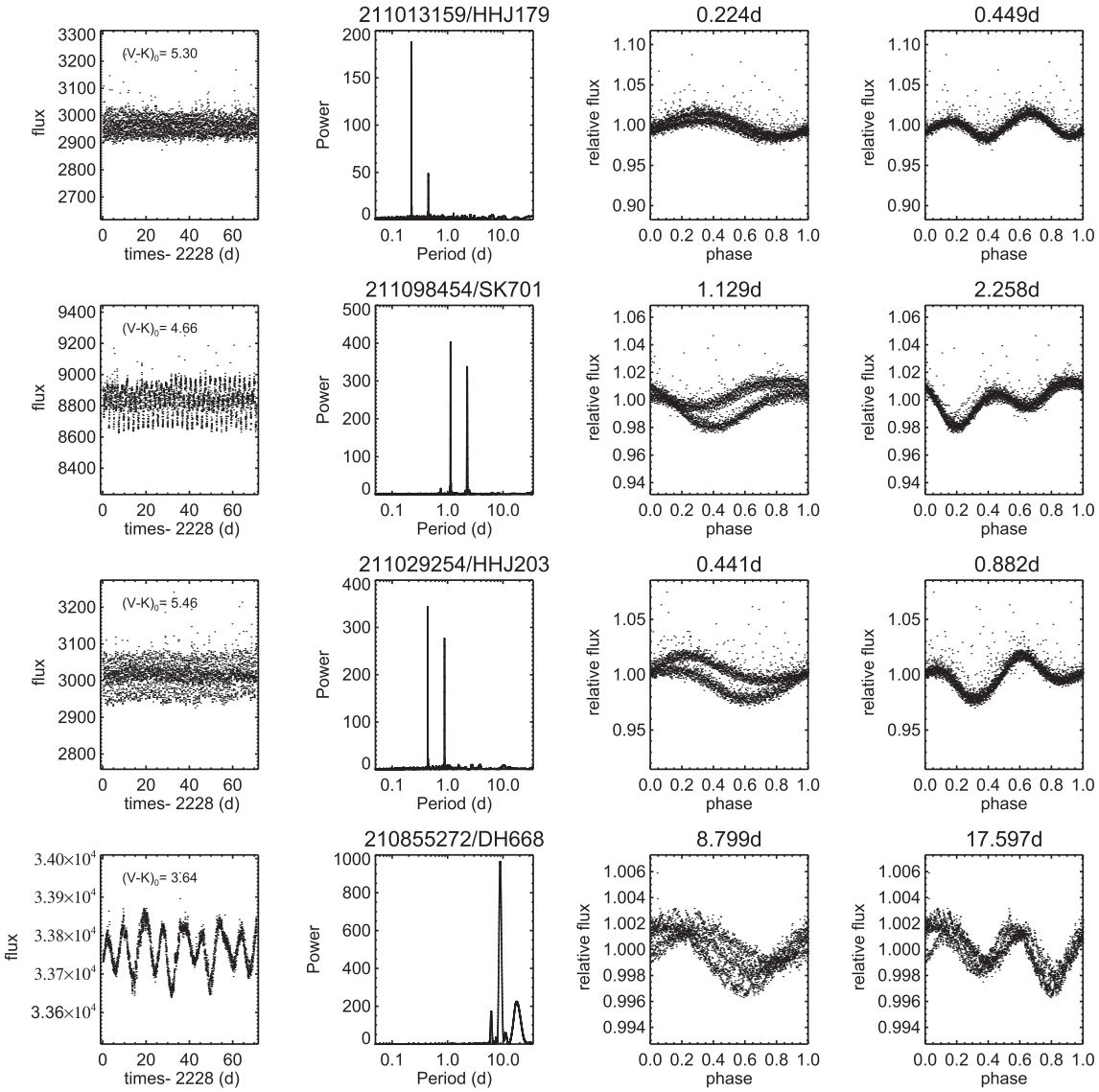

Figure 1. Four examples of the double-dipped category, where the double-dipped structure in the LC "fools" the periodogram such that the maximum peak in the periodogram is half the true period. First column: full LC (with $(V - K_s)_0$ for star as indicated); second column: LS periodogram; third column: phased LC with P corresponding to the maximum peak in the periodogram; fourth column: phased LC, with best period (in days) as indicated. Rows, in order: EPIC 211013159/HHJ 179, 211098454/SK 701, 211029254/HHJ 203, and 210855272/DH 668. These are representatives from a range of brightnesses and periods. In these cases, the double-dipped structure redistributes power from P into $P/2$ because the dips are of comparable depth. These LCs most likely result from stars with two spots or spot groups on well-separated longitudes. (NB: 210855272/DH 668 is discussed in Paper I, because the longer period identified here makes it an outlier in the P vs. $(V - K_s)_0$ plot, but the shorter period would move it "into line" with other stars of its $(V - K_s)_0$. However, we believe that the longer period is correct for this star.)

Those that show movement of one dip/hump with respect to the other over the *K*2 campaign could be explained by spot/spot group formation or migration with strong latitudinal differential rotation. Those that do not show such changes, therefore, are more likely to be rotating as solid bodies, or at least have weaker latitudinal differential rotation and/or more spot stability. Although there is a huge range of P for moving and stationary double-dip objects, the moving double-dip objects are on the whole rotating slower than the stationary double-dip objects. Faster rotation should yield a more dipolar magnetic field and more stable spots/spot groups; see discussion in Paper III. This is consistent with the results from Zeeman-Doppler imaging of M dwarfs (Morin et al. 2008, 2010).

3.2. Beating LCs

About 16% of the sample (18% of the periodic sample) has obvious signatures of beating in the LC, such as changes in the envelope over the campaign; see Figure 3. Most of those have some combination of obvious beating in the LC and multiple frequencies in the periodogram (but are not the double-dip phenomenon above). For these, phasing to the maximum peak in the periodogram does not show a very well-phased LC, because of the structure provided by the subsidiary peak(s). Phasing the LC at the subsidiary peak(s) shows similar coherence (or lack thereof) for the same reason, even when the FAP is low.

We identified LCs with these kinds of properties initially by eye based on structure in the LC or in the power spectrum. We

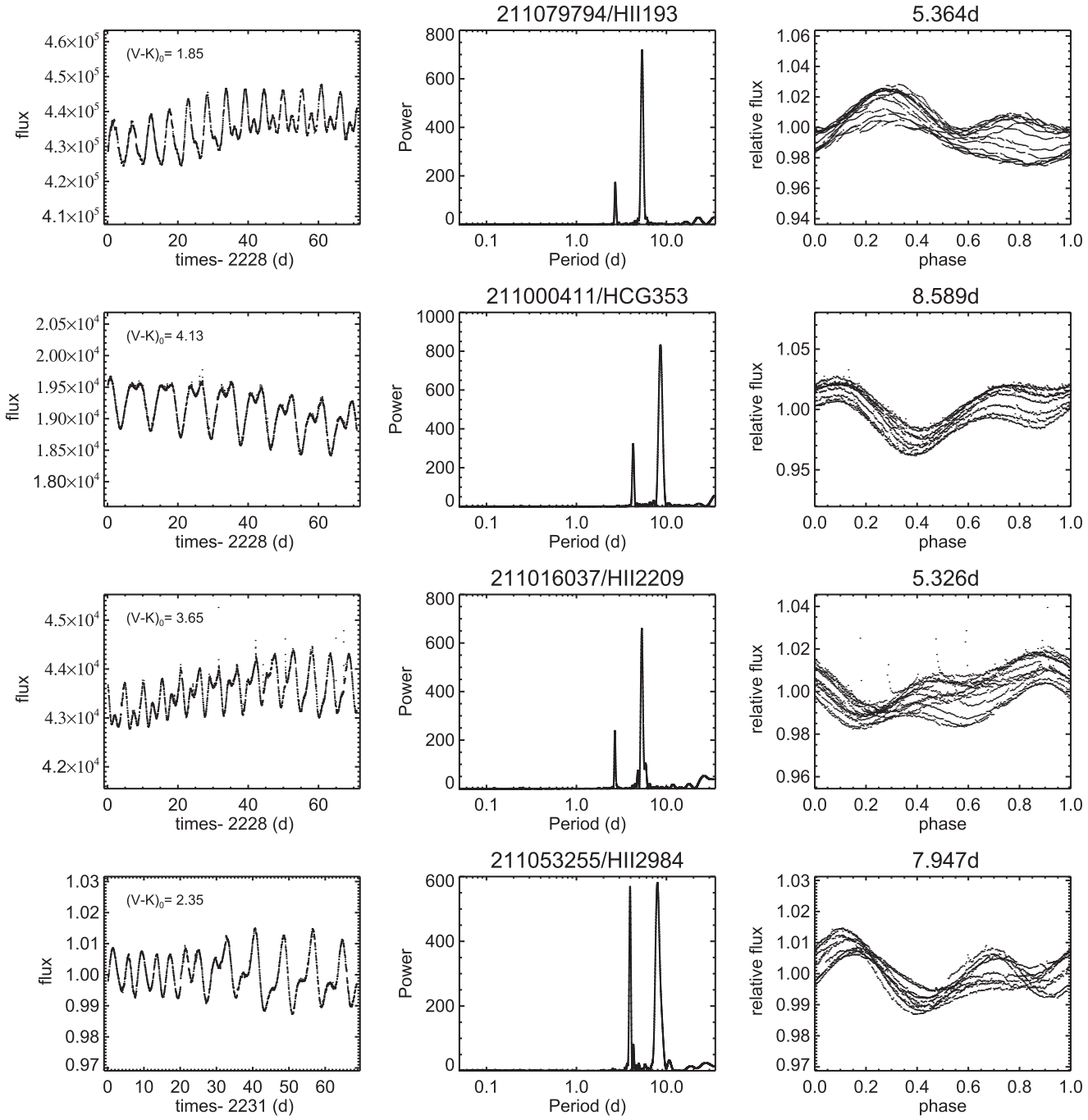

Figure 2. Four examples of the moving double-dipped category, where there is a double-dipped structure in the LC, as in the prior figure, but there are visible changes in the relative locations of the structure over the campaign. First column: full LC (with $(V - K_s)_0$ for star as indicated); second column: LS periodogram; third column: phased LC, with best period (in days) as indicated. Rows, in order: 211079794/HII193, 211000411/HCG 353, 211016037/HII 2209, and 211053255/HII 2984. These LCs most likely result from stars with two spots or spot groups at different latitudes with differential rotation and/or spot evolution. Also see Section 3.5.

then performed an additional LS periodogram analysis with much finer frequency sampling than our initial approach, but only between $P/3$ and $3P$, for the period with the maximum power. We noticed primarily two kinds of periodogram structure. One kind has a measurably wide primary peak, and/or an asymmetric primary peak. The other kind has peaks that are very narrow, and the main power peak breaks into two (or sometimes more) resolved components. Often a secondary peak that appeared at first glance to be a harmonic is not, in fact, a true harmonic of the main peak. Sometimes the multipeaked or asymmetric structure seen in the main peak can also be found in its harmonic (see below and Figure 3).

We discuss the complex power spectrum peaks and those with resolved multiple frequencies in the next two subsections, respectively. We note, however, that in a few cases, the LC is seen to have a beating structure, but the components are not resolved in the power spectrum; that is, the peak is still thin, and no other significant peaks are noted. In a few cases, it seems that the *frequency* is not changing, but the *amplitude* of one or both of the signals is changing. In the remainder of the cases, it seems that the periods are so close together that the

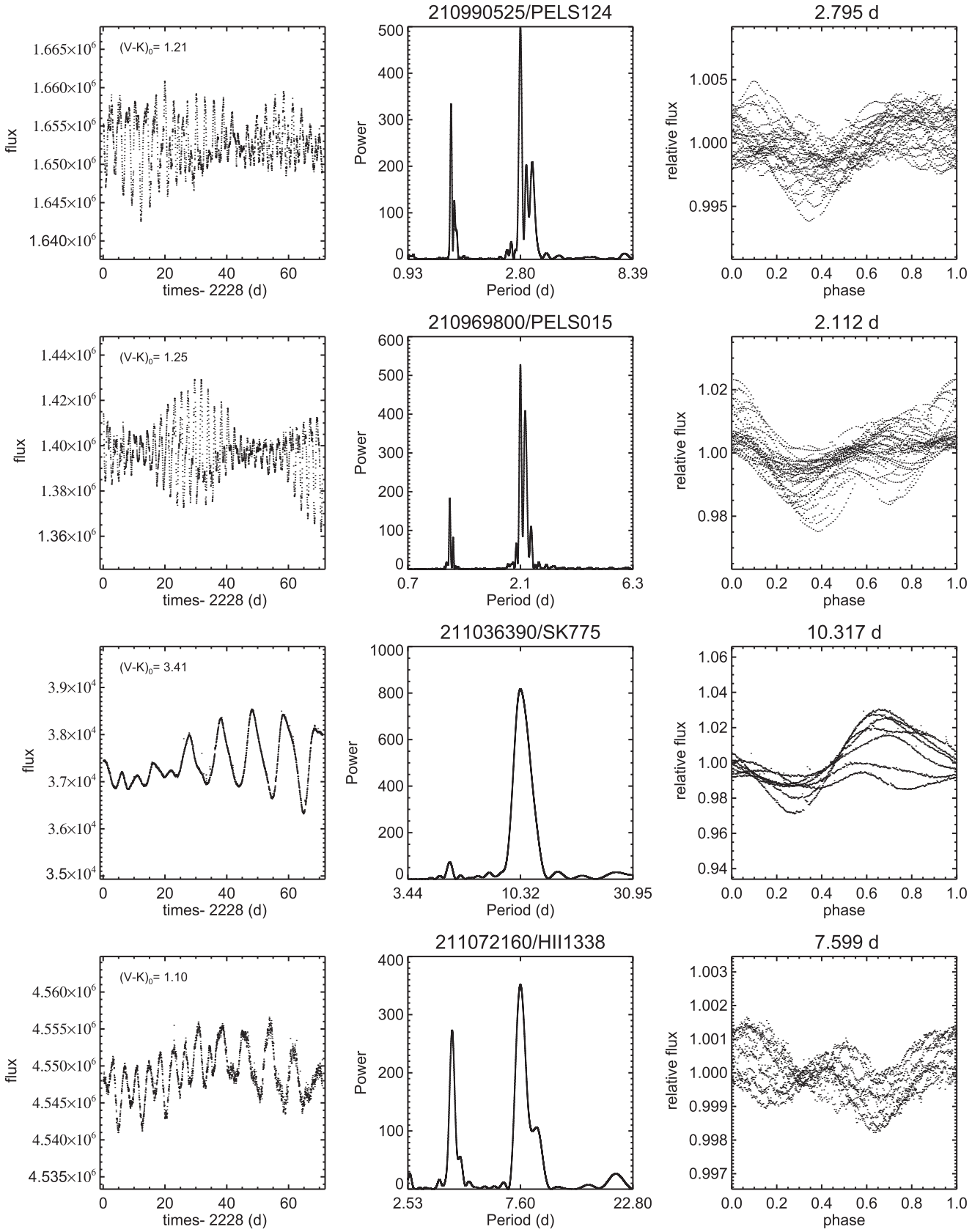

Figure 3. Four examples of the beater and complex peak categories. Beating is seen in the LC, and for these examples, the peak in the periodogram is complex, broad, and/or structured. Left column: full LC (with $(V - K_s)_0$ for star as indicated); middle column: periodogram; right column: phased LC for maximum peak. Rows, in order (with the periods corresponding to significant peaks in parentheses): 210990525/PELS 124 (2.795, 1.421, 3.330), 210969800/PELS 015 (2.112, 2.212), 211036390/SK 775 (10.317), and 211072160/HII 1338 (7.599, 8.899). Note that the power spectrum shows peaks of measurable width and/or multiple peaks. Sometimes the multipeaked structure can be found in both the main peak and its harmonic. These LCs are likely a result of latitudinal differential rotation and/or spot evolution.

72 day campaign does not provide enough cycles to distinguish the periods.

When the LC looks "beating," and/or there are complex power spectrum peaks, there are three possible interpretations: (a) spots or spot groups evolving; (b) latitudinal differential rotation from spots/spot groups at more than one latitude during the *K*2 campaign; (c) spot-modulated periods from two (or even three) unresolved stars in the *K*2 aperture. The majority of the stars identified as beaters are the earlier types, $(V-K_s)_0 \lesssim 4$, which is where strong latitudinal differential rotation is expected. However, hotter stars have shorter-lived spots in general, so spot/spot group evolution may also be important.

3.3. Complex, Structured Peaks and Unresolved Multiperiod Peaks

To find objects where the peak(s) in the periodogram are distinctly broad and/or structured, we took multiple approaches; examples are shown in Figure 3. About 11% of the sample (12% of the periodic sample) falls into this category of complex, structured peaks and unresolved multiperiod peaks.

First, for all of these objects, we computed a power spectrum with finer frequency resolution, as discussed above. If the maximum peak is clearly asymmetric (such as seen in the first and last rows of Figure 3), then we added the star to this category on the basis of having "complex, structured peaks." If the higher frequency resolution power spectrum incompletely resolves the peak into pieces (as seen in the second row of Figure 3, where the wings of the peaks run into each other at power levels >0), then we added the star into this category on the basis of having a "complex peak."

Finally, to assess whether or not the peak is broader than expected for its period, we took the FWHM of the actual peak (*not* the FWHM of, say, a Gaussian fit to the peak, but the true FWHM of the peak) and plotted that as a function of period. For most of the sample, this relationship falls on a line when plotted in log–log space.[21] We fit the line, subtracted it from the distribution, and looked for things that deviated significantly from 0. This is not a good approach for identifying, say, objects like the first and last rows in Figure 3, because the additional structures seen near the base of the peaks do not affect the half maximum. However, the object in the third row of Figure 3 has a peak much broader than expected for stars with single periods near 10.3 days. This is the final type of object added to this "complex peak" category—those with peaks wider than expected for that period. In these cases, the period (and/or amplitude) is changing over the campaign, and/or the multiple periods are so close together that the power spectrum cannot resolve them.

These kinds of power spectra are very suggestive of latitudinal differential rotation and/or spot evolution. Periods that are very close together and/or changing over the *K*2 campaign could easily be explained if we are seeing spots at different latitudes in a differentially rotating star, either spots that persist over the *K*2 campaign or spots that appear, disappear, or otherwise change over the *K*2 campaign. The majority of the stars identified as having complex peaks are the earlier types, $(V-K_s)_0 \lesssim 4$, which is where strong latitudinal differential rotation is expected, but also where spots may most rapidly evolve. Stars where the complex peak structure of the primary peak is repeated in the first harmonic may be more likely to be differential rotation than spot evolution. On the other hand, complex peaks close to the rotation period can also arise when active regions appear and decay at random longitudes, giving brief periods of coherent modulation with phase shifts between them. The sine function used in the periodogram interferes constructively with such widely separated but phase-shifted modulations at a frequency slightly different from the true rotation frequency. For a finite data train lasting a few active-region lifetimes, this splits the fundamental into several shifted peaks, even in the absence of differential rotation.[22] We (A.C.C. and S.A.) have successfully simulated these LCs as a Gaussian process with a covariance function comprising a single modulation period and a spot lifetime of a few rotations. The shapes of the resulting LCs resemble these LCs closely, and the pattern of splitting of their periodogram peaks is very similar.

3.4. Resolved Multiperiod

In some cases, there are well-resolved, very narrow peaks in the power spectrum and both periods are real; see Figure 4. The periods need not be very close together and they are not harmonics, though sometimes the harmonics appear (first row of Figure 4). About 20% of the sample (22% of the periodic sample) falls into this category of resolved periods.

We wished to differentiate situations as in the second row of Figure 4, where the peaks are very close together, and situations as in the last row of Figure 4, where the peaks are substantially farther away from each other. For every situation in which we had at least two viable periods for a star, we took the closest two periods out of those detected, subtracted the smaller from the larger, and divided by the primary peak. The primary peak is the strongest in the power spectrum, and what we take to be the rotation period of the primary star in the system, but may or may not be one of the two closest peaks. If that metric, $\Delta P/P_1$, is less than 0.45, then we take it to be resolved close peaks; if that metric is greater than 0.45, then we take it to be resolved distant peaks. This dividing line of $\Delta P/P_1 = 0.45$ was determined by inspection of the LC and periodogram properties, as well as the morphology of the $\Delta P/P_1$ distribution; see much more discussion in Section 6.

Of the ~20% of the sample that falls in this broader category of resolved peaks, 73% are tagged close, and 30% are tagged distant. Note that some objects have both close and distant peaks. Both resolved close and resolved distant periods are found at all $(V-K_s)_0$; the distant periods are equally likely at all $(V-K_s)_0$, but the close periods are slightly more frequent (as a fraction of the sample) for $(V-K_s)_0 \lesssim 3.7$.

Particularly for the stars with $(V-K_s)_0 \lesssim 3.7$ and having resolved close periods, we suspect that these are another manifestation of latitudinal differential rotation and/or spot evolution. For the resolved distant periods, we suspect that they are binaries, where the two different periods are the different rotation rates of the components of the binary. For ~60% of the stars in this category, there is at least some evidence that it is a binary or there is more than one star in the *K*2 aperture; for the

[21] The expected peak width (where f is frequency) is $df \sim 1/T$ (where T is the total length of the campaign), which is independent of period, and consequently $dP = df \times P^2$.

[22] There is a close analogy with the collisional spectral-line broadening that results from phase changes induced by atomic collisions in a gas.

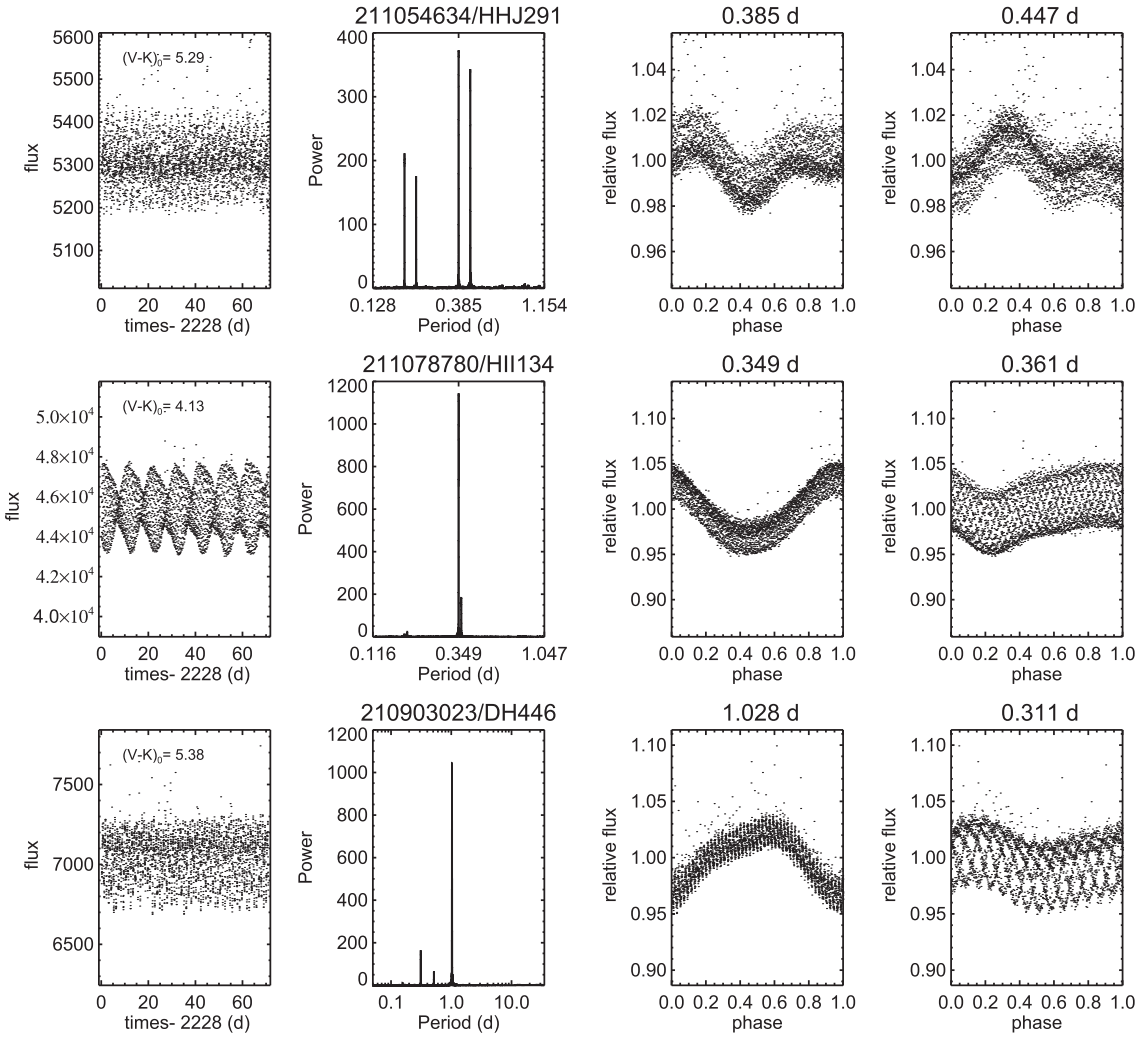

Figure 4. Three examples of the resolved peak categories, LCs where there are two distinct, well-resolved frequencies. First column: full LC (with $(V - K_s)_0$ for star as indicated); second column: periodogram; third column: phased LC for primary peak; fourth column: phased LC for secondary peak. Rows, in order (with the periods corresponding to significant peaks in parentheses): 211054634/HHJ 291 (0.385, 0.447; $\Delta P/P_1 = 0.162$), 211078780/HII 134 (0.349, 0.361; $\Delta P/P_1 = 0.035$), 210903023/DH 446 (1.028, 0.312; $\Delta P/P_1 = 0.698$). Note that the power spectrum shows multiple, resolved peaks. Following the $\Delta P/P_1$ metric divisions, the first and second have resolved close periods (the two peaks are very close together in the periodogram), and the third has resolved distant peaks. All three of these have companions that can be seen in POSS or Robo-AO data, so these LCs are likely to result from binaries, with one period per star.

rest, there is no information suggesting binarity, but in many cases, this may reflect simply a lack of data.

3.5. Shape Changers

There is a category of LC where the power spectrum suggests that there is just one period derived from the data, but there are visible, substantial changes in the shape of the LC over the campaign. These so-called shape changers are ∼14% of the sample (∼15% of the periodic sample).

Examples are seen in Figure 5 (also see Figure 2 for the moving double-dips, which are also shape changers). Sometimes the overall envelope of the LC changes, manifesting as changes in shape of the phased LC. In other cases, one can see additional structure appear in the LC and grow in strength, or even move with respect to the other structures in the LC over the course of the campaign.

Spot evolution seems like a likely physical interpretation; one can imagine a new spot or spot group appearing or disappearing over the campaign to create these LCs. For those where structure in the LC moves with respect to other structures in the LC, spot evolution combined with latitudinal differential rotation could explain the observations. We note, though, that there are other LC categories where we find two or more periods that we attribute to latitudinal differential rotation and/or spot evolution. In the case of shape changers, the changes are evidently happening more slowly, such that there are not enough rotation periods (and/or stability in the periods), and so an additional period cannot be resolved. If we were able to obtain LCs over more than 72 days, perhaps a second (or third) period could be derived, in which case some of these stars could end up in the "complex peaks" and/or "beater" categories above.

The shape changers have $1 \lesssim (V - K_s)_0 \lesssim 5$. While the $(V - K_s)_0$ range for shape changers overlaps that for beaters and complex peaks, the shape changers extend to redder $(V - K_s)_0$; see additional discussion below and in Paper III. About 60% of the shape changers are also in another category described above.

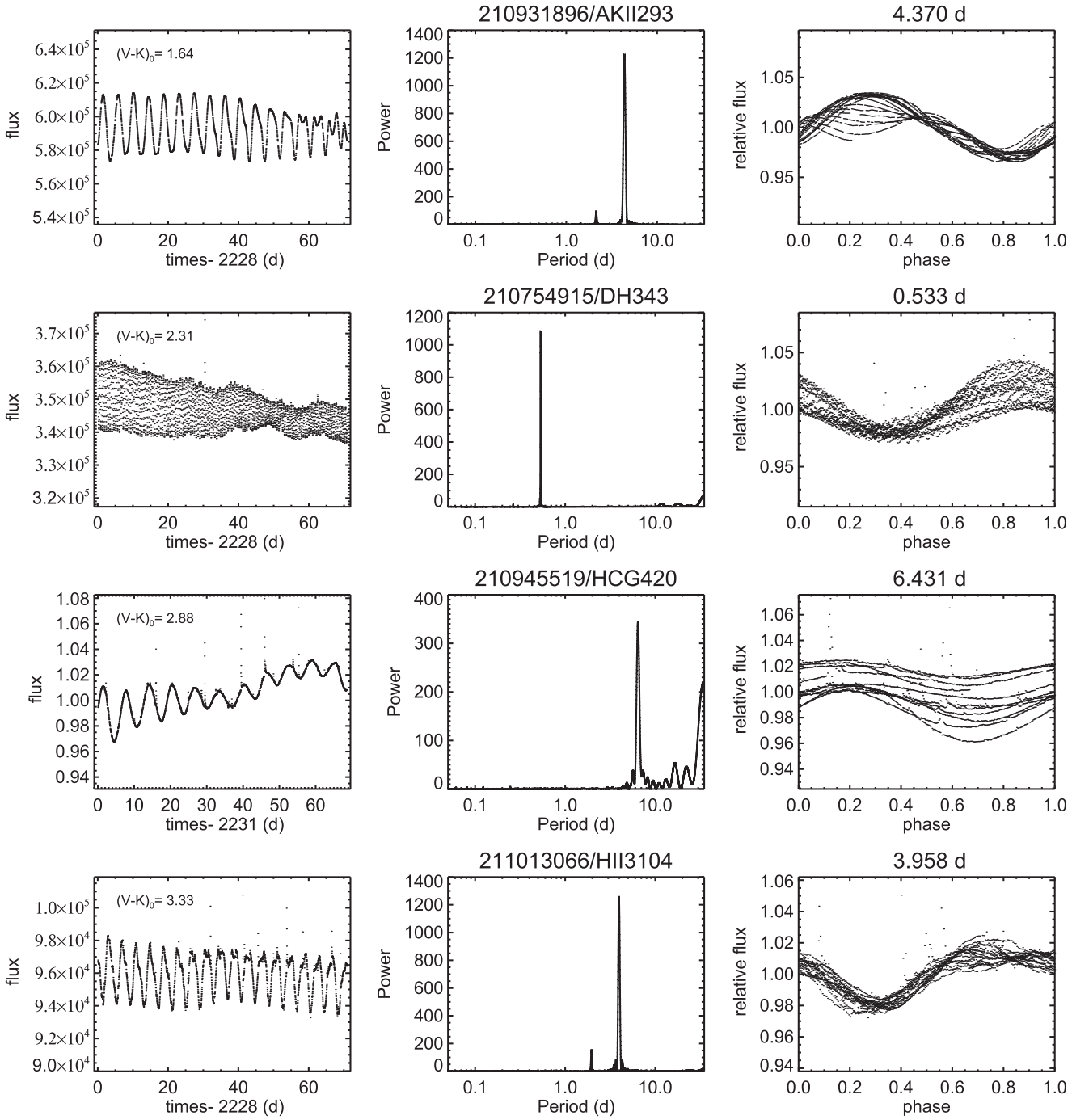

Figure 5. Four examples of the shape changer category, LCs where there are changes in the shape of the LC over the *K*2 campaign. Left column: full LC (with $(V - K_s)_0$ for star as indicated); middle column: periodogram; right column: phased LC for maximum peak. Rows, in order: 210931896/AKII 293, 210754915/DH 343, 210945519/HCG 420, 211013066/HII 3104. Note that the power spectrum shows a single peak, but the shape changes over the campaign. Assuming that these shapes are a result of spot evolution, sometimes it looks like a new spot or spot group is appearing or disappearing over the campaign. It is likely that if we had a longer campaign, then these objects would be instead in one of the complex peak/resolved peak categories, but 72 days is not long enough to distinguish the frequencies.

3.6. Orbiting Clouds?

In six cases, the period we identify in the power spectrum yields a phased LC of unusual shape; see Figure 6. The phased LCs show shallow, angular dips (highlighted with arrows in Figure 6) that cover a relatively small portion of the total phase. The pattern is stable (or nearly stable) over the 72 day *K*2 campaign. In several cases, the LCs also show broad dips, which presumably are due to cool spots on the stellar surface. Half of these stars have an additional secondary period. Four are high-quality members, one is a lower-quality member (211013604/HCG 332), and one is a probable non-member (211144341/BPL 300). About 0.6% of the sample (0.7% of the periodic sample) has these structures.

The narrowness of the highlighted dips seems impossible (or at least very difficult) to explain with cool spots. A Fourier decomposition of a starspot LC has essentially no power beyond the second harmonic. Foreshortening and limb darkening conspire to ensure that for spots there are never more than two humps per

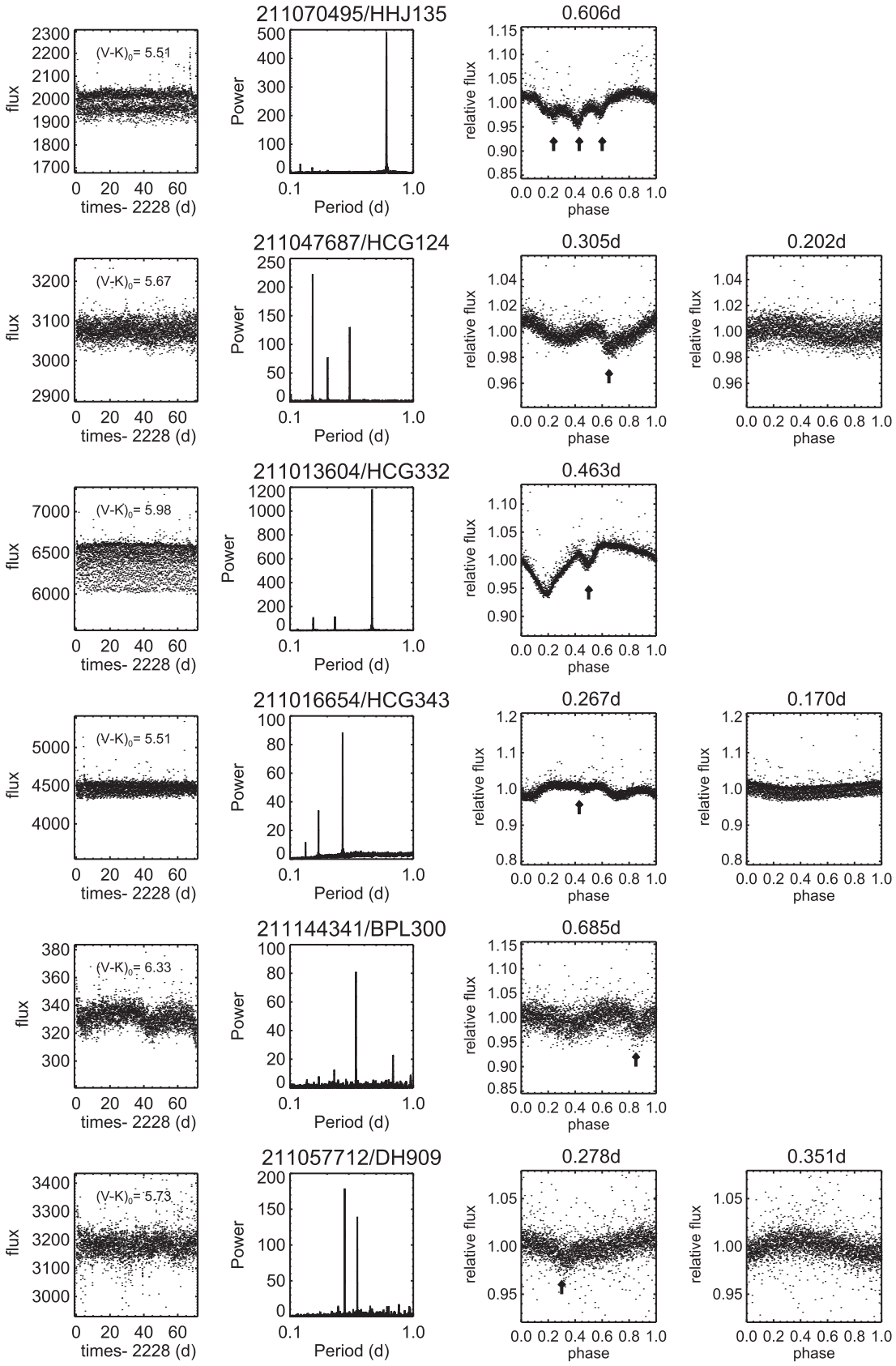

Figure 6. All six stars identified as having repeated, angular, brief dips in their LCs. First column: full LC (with $(V - K_s)_0$ for star as indicated); second column: periodogram; third column: phased LC for maximum peak; fourth column: phased LC for secondary peak, if present. Rows, in order: 211070495/HHJ 135, 211047687/HCG 124, 211013604/HCG 332, 211016654/HCG 343, 211144341/BPL 300, 211057712/DH 909. Arrows in the first phased LC indicate the shallow, angular dips discussed in Section 3.6. These LC structures may be due to orbiting clouds or debris.

LC. The variations in these stars are too rapid to be fitted with a linear combination of P, $P/2$, and $P/3$. However, these dips are also too broad to be due to transits of secondary stars or giant planets. The basic information for these stars is all in Table 2; all of them are fairly late M dwarfs, and all have periods <0.7 days, which means they have fairly normal periods for Pleiades stars of this mass.

We have identified two possible physical explanations for the shallow dips in these LCs. First, they could be due to eclipses of warm, dense circumstellar clouds formed near the top of large coronal loops and temporarily held near the Keplerian corotation radius by centrifugal force (Collier Cameron 1988; Collier Cameron & Robinson 1989). Such clouds have been identified in synoptic spectra of several rapidly rotating, young dwarfs (e.g., AB Dor), though not previously in time series photometry. For at least four of the six stars, the cloud associated with the narrow dip would be located near the corotation radius since the periods for the narrow and broad dips are apparently the same, or nearly the same. In two cases, the narrow dip appears to move slightly in phase relative to the broad dip or to another narrow dip; differential rotation is very unlikely in these stars, given their spectral type and rotation rate. To see slingshot prominences in broadband photometry, we would have to be observing eclipses of continuous bound-free emission as the cloud passes behind the star. For this reason, we would only expect to see the phenomenon easily in rapidly rotating stars with very low photospheric surface brightnesses, i.e., late M dwarfs.

The other possible physical mechanism for the narrow dips is that they could be due to comets or some other form of "debris" orbiting these stars, perhaps similar in some respects to stars from the main *Kepler* field recently found to show transient, shallow flux dips (Vanderburg et al. 2015; Boyajian et al. 2016). In this case, the dips would be associated with transits of these dusty structures in front of the star. It is not obvious why material would be located near the Keplerian corotation radius so frequently in this model.

If these objects have orbiting particulate debris, one might expect an IR excess from the debris. However, none of these objects have truly compelling evidence for an infrared (IR) excess; the longest-wavelength detection for any of them is WISE-3, 12 μm, which is detected in four of the six stars. The most likely excess is found in 211013604/HCG 332, which has [3.4]–[12] = 0.53 mag, and the metric often used to assess signficance of excess, $\chi = ([3.4] - [12])/\sqrt{\sigma^2_{[3.4]} + \sigma^2_{[12]}}$, is 5, so not very obvious. The other stars with 12 μm detections have similar-sized [3.4]–[12] but less significant χ. Moreover, only a small fraction of dust could account for these dips; see, e.g., Gillen et al. (2014), Terquem et al. (2015), and Gillen et al. (2016). Further investigation is warranted, such as monitoring in different wavelengths and a more careful assessment of any small IR excesses.

HCG 332 is one of two stars originally made famous in Oppenheimer et al. (1997). This work reported results of a search for lithium in very low mass members of the Pleiades; they were attempting to identify stars at the lithium depletion boundary marking the point cooler than which Pleiades-age stars have not reached core temperatures hot enough to burn lithium. Oppenheimer et al. found no stars fitting the criteria to be at the lithium depletion boundary, but they did identify two purported, somewhat higher-mass Pleiades M dwarfs that had strong lithium features when no lithium should be present. (The other star is HCG 509, discussed in the Appendix of Paper I.) Both stars are located >1 mag above the Pleiades single-star main sequence, which they interpreted to mean they are very young pre-main-sequence stars and not Pleiades members. We will report elsewhere on the implications for models of these two stars based on their $K2$ light curves and additional spectroscopy (D. Barrado et al. 2016, in preparation).

3.7. Pulsators and Rotation

Throughout most of the mass range of interest to this paper, rotational modulation due to starspots provides the only plausible physical mechanism to explain the periodic LCs we see. However, at the high-mass end of our sample ($(V - K_s)_0 \lesssim 1.3$, $M \gtrsim 1.2\,M_\odot$), pulsation may provide an alternative explanation.

In eight cases (~1% of the sample), the power spectrum reveals a "forest" of significant (FAP = 0) peaks in the periodogram, all at very short periods; see Figure 7 for examples and Table 3 for a list of these stars. They are also all very small amplitude LCs (median 0.0027 mag). In most cases, these must be pulsators; if interpreted as rotation periods, the period would exceed the breakup limit. They are all earlier types—their $(V - K_s)_0$ ranges from 0.24 to 0.85 (mid-A to early F). Five of the eight stars we have identified in this category have periods $\lesssim$0.1 days; the other three are all ~0.3 days and include both the bluest and reddest $(V - K_s)_0$ of this category (spectral types A1, A2, and A9; see Table 3).

Delta Scuti stars have spectral types A or F and periods typically $\lesssim$0.3 days (e.g., Breger 1979). They are lower-mass Cepheid analogs. Several of the Pleiades with $K2$ LCs have been identified in the literature (Breger 1972; Fox Machado et al. 2006) as being δ Scuti pulsators, but most of them are too bright for us to reliably identify a period at all with the LC versions we have, much less a pulsator-type power spectrum. Two of them are ones we identified as pulsators, and the rest are very bright; see Table 3. For two of these bright stars, knowing that they are thought to be pulsators, one can find the likely relevant peaks in the power spectrum in among the noise, but the LC is significantly compromised and we did not identify these periods a priori.

We suspect that the remaining stars we identified as likely pulsators are also δ Scutis, particularly the three with the shortest periods. The other three near ~0.3 days are at the outer edge of the accepted range for δ Scuti periods, as well as the outer edge of the expected spectral type range. However, given the spectral types for the stars already in the literature as δ Scutis (see Table 3), perhaps the spectral type range for these pulsators is not so rigidly defined. We thus identify all six of our a priori identified pulsators as δ Scutis. No modern $v \sin i$ values are available for these stars in the literature.

The δ Scutis are relatively easily identified due to their very short periods that essentially cannot be ascribed to rotation because the inferred rotational velocities would exceed breakup. However, another type of pulsating variable is the γ Dor type (e.g., Krisciunas 1994; Kaye et al. 1999), which may have the same underlying physics as δ Scutis (e.g., Xiong et al. 2016). Gamma Dors are also A or F stars, but are pulsating with on average longer periods, ~0.4–3 days (e.g., Balona et al. 1994; Kaye et al. 1999). These are harder to distinguish from rotation periods, because their periods overlap with expected spot-modulated rotation periods for their masses.

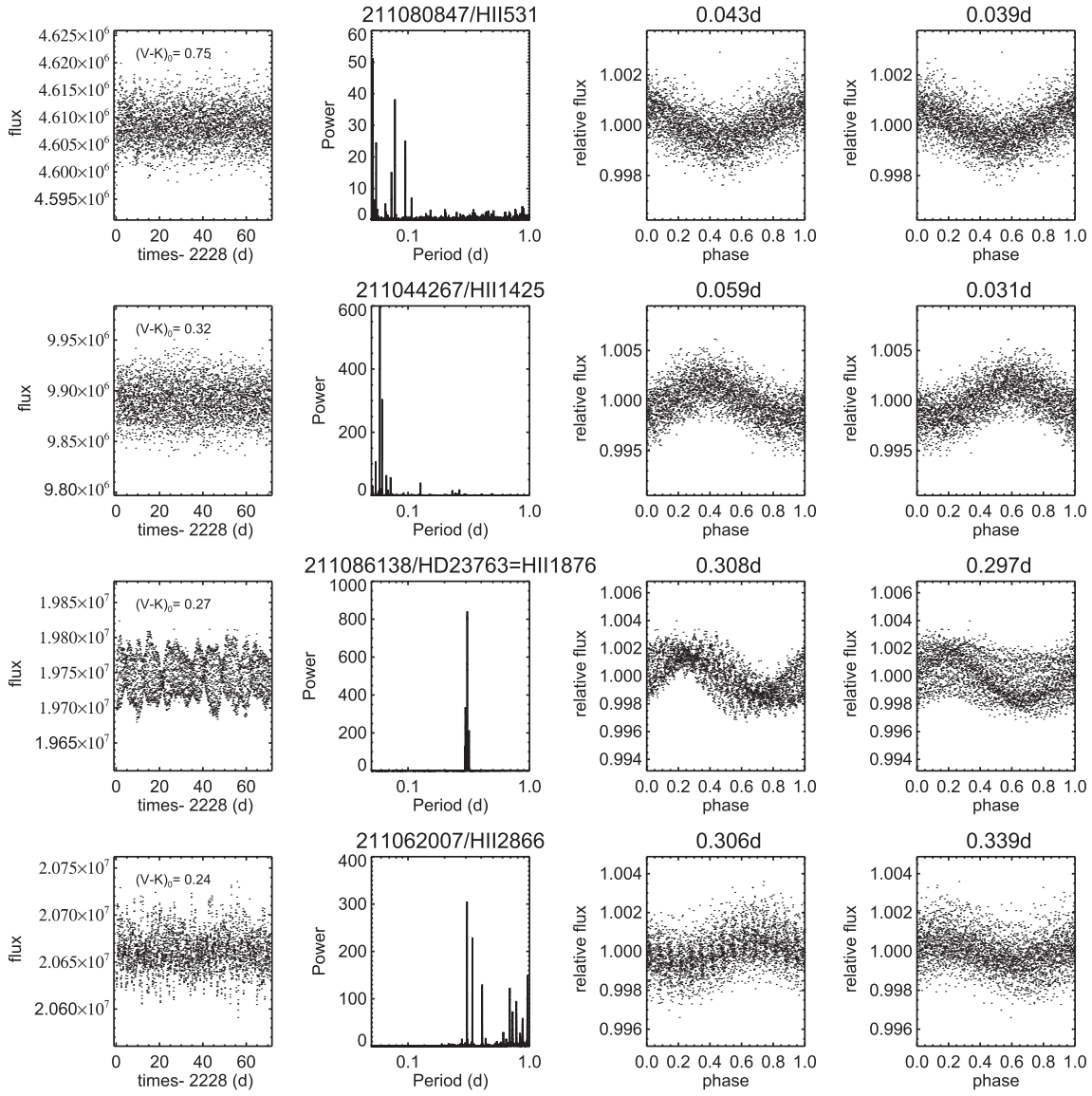

Figure 7. Four examples of the pulsator category, stars that are likely δ Scuti pulsators. First column: full LC (with $(V - K_s)_0$ for star as indicated); second column: LS periodogram; third column: phased LC at the P with the highest peak in the periodogram; fourth column: phased LC at the P with the second-highest peak in the periodogram. Rows, in order: EPIC 211080847/HII 531, 211044267/HII 1425, 211086138/HD 23763 = HII 1876, 211062007/HII 2866.

It has been shown that for stars identified as γ Dors in the main *Kepler* field, the measured periods correlate well with $v \sin i$ values for those stars (Balona et al. 2011) and similarly for γ Dors not necessarily in the *Kepler* field (Kahraman Alicavus et al. 2016). This suggests that it might be difficult to discriminate between pulsation and rotation as the drivers of the observed variability for at least some of our F stars. In fact, Balona et al. (2011) acknowedge that many of the stars they identify as γ Dor variables in the main *Kepler* field may instead owe their variability to rotation and starspots. Bradley et al. (2015), despite selecting targets specifically to look for γ Dor and δ Sct stars in the instability strip in the *Kepler* field, find that 74% of their sample is better interpreted as spot modulation.

Our close resolved and/or complex peak categories contain many power spectra that resemble those of γ Dors from the main *Kepler* field in Balona et al. (2011), but ours extend over a much wider range of color than for just near the instability strip, down to $(V - K_s)_0 \sim 4$ for the complex peaks alone. There is no clear separation of the LC characteristics of these stars from slightly more massive or less massive stars; instead, there is simply a smooth transition. There exist stars with this LC/periodogram morphology both redward and blueward of the boundaries that are expected to define the γ Dor class. Figure 8 includes the LCs and periodograms for some of the stars with γ Dor-like variability. There is a measured $v \sin i$ for each of those stars; for the measured P, the measured $v \sin i$ should be ~20–30 km s^{-1}, which they are. For this paper, we choose to adopt the dominant LS period as the rotation period for all of these stars. Given the good correlation between $v \sin i$ and period found by Balona et al. (2011) and Kahraman Alicavus et al. (2016), this period is unlikely to be very far from the true rotation period even if pulsation is the actual cause. Based on the wide spectral type range over which we see this type of variability and the smooth change in LC morphology as one traverses the G to F star spectral range, we believe that it is likely that rotation is the correct physical mechanism to explain these kinds of LCs and periodograms, particularly for the ones with $(V - K_s)_0 > 1.1$.

Table 3
Pulsators

EPIC	Other Name	SpTy	Notes
211018096	HD 23791 = HII 1993	A8	Identified a priori by us as a pulsator, $P \lesssim 0.1$ days; obvious δ Scuti
211044267	HII 1425	A3V	Identified a priori by us as a pulsator, $P \lesssim 0.1$ days; obvious δ Scuti; literature-identified δ Scuti (Breger 1972; Fox Machado et al. 2006); in Figure 7
211057064	HD 23863 = HII 2195	A7V	Identified a priori by us as a pulsator, $P \lesssim 0.1$ days; obvious δ Scuti
211066615	HII 652	A3V	Identified a priori by us as a pulsator, $P \lesssim 0.1$ days; obvious δ Scuti
211080847	HII 531	A9m[a]	Identified a priori by us as a pulsator, $P \lesssim 0.1$ days; obvious δ Scuti; in Figure 7
211062007	HII 2866	A2V	Identified a priori by us as a pulsator, $P \sim 0.3$ days; likely δ Scuti; in Figure 7
211086138	HD 23763 = HII 1876	A1V	Identified a priori by us as a pulsator, $P \sim 0.3$ days; likely δ Scuti; in Figure 7
211093705	HII 697	A9	Identified a priori by us as a pulsator, $P \sim 0.3$ days; likely δ Scuti; literature-identified δ Scuti (Breger 1972)
211115721	HII 1266	A9V	Literature-identified δ Scuti (Fox Machado et al. 2006), not identified by us, for which we have just one (long) period
211072836	HII 1362	A7	Literature-identified δ Scuti (Fox Machado et al. 2006), not identified by us because star too bright
211088007	HII 158	A7V	Literature-identified δ Scuti (Fox Machado et al. 2006), not identified by us because star too bright (though knowing that it is a pulsator, one can identify the likely relevant periodogram peaks)
211101694	HII 1384	A4V	Literature-identified δ Scuti (Fox Machado et al. 2006), not identified by us because star too bright (though knowing that it is a pulsator, one can identify the likely relevant periodogram peaks)

Note.
[a] All of the spectral types here come from Mendoza (1956), except for HII 531, which Mendoza (1956) lists as "Am?," but Gray et al. (2001) give a more definitive A9m.

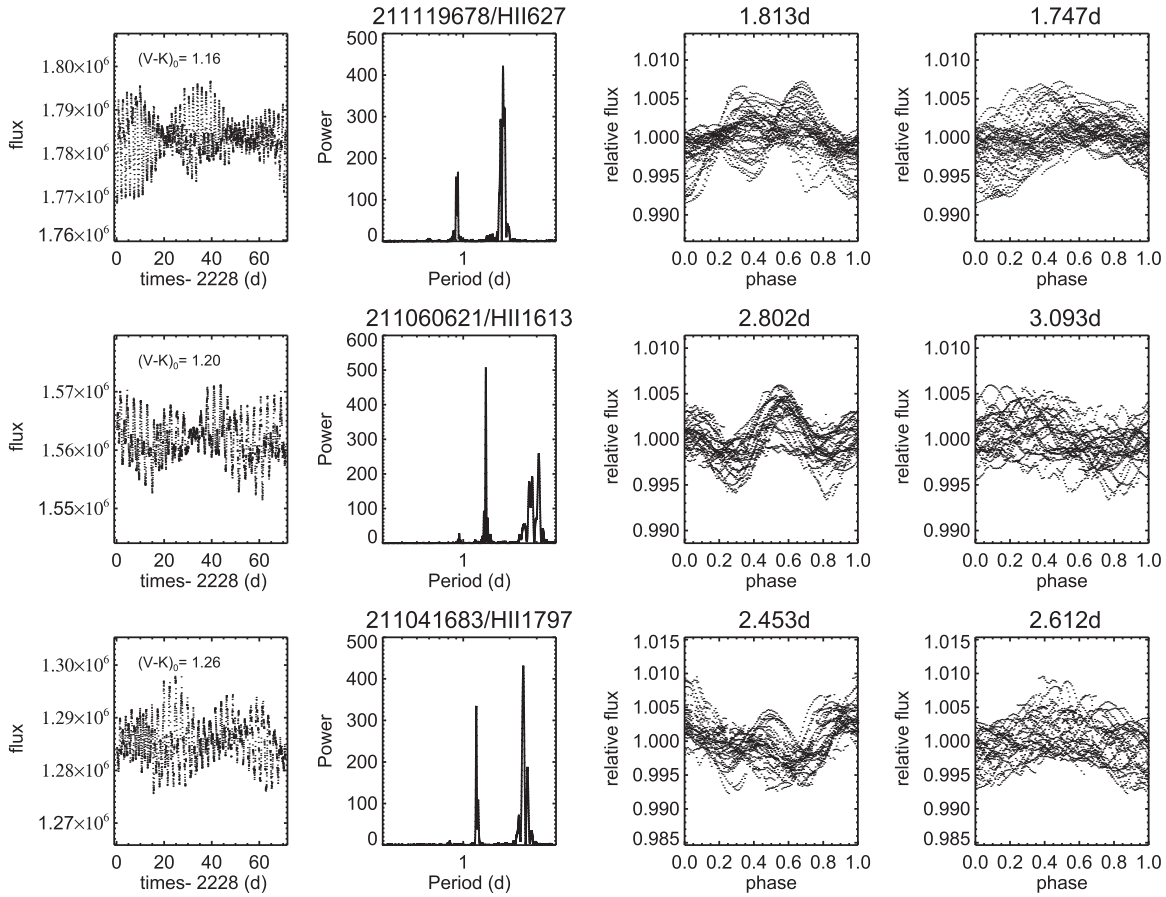

Figure 8. Examples of objects that may be γ Dors. First column: full LC (with $(V - K_s)_0$ for star as indicated); second column: periodogram; third column: phased LC for primary peak; fourth column: phased LC for secondary peak. Rows, in order: 211119678/HII 627, 211060621/HII 1613, 211041683/HII 1797. The measured $v \sin i$ from the literature is ~33, 20, and 20 km s^{-1}, respectively, which is consistent with these being rotation rates. 210990525/PELS 124 from Figure 3 may also be in this category. (Its $v \sin i \sim 20$ km s^{-1} as well.)

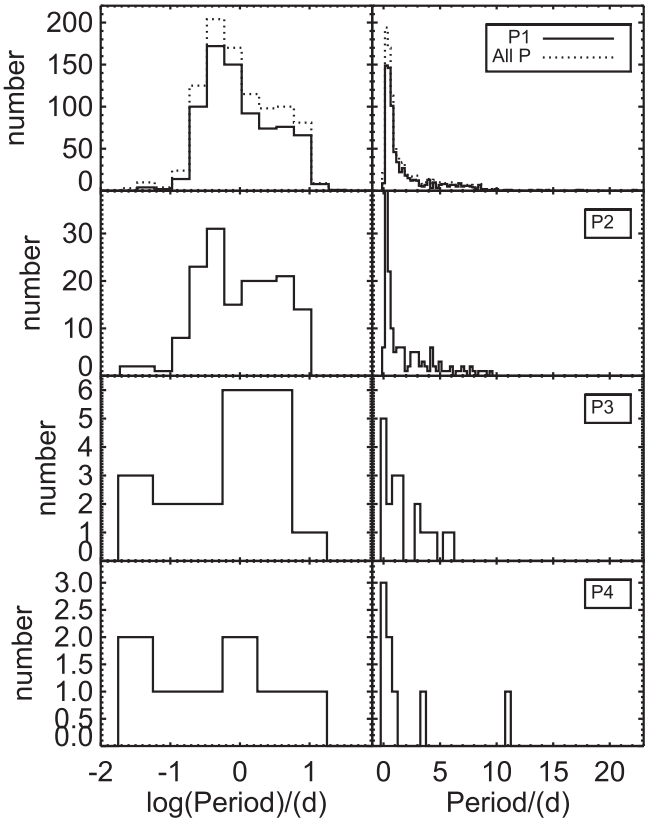

Figure 9. Histograms of the periods found by our analysis, in days. The left column contains histograms of the log (P), and the right column contains histograms of linear P. In the first row, the solid line is the primary period (that which we take to be the rotation period of the star), and the dotted line is (for reference) a histogram of *all* the periods found here, including the secondary, tertiary, and quaternary periods. The second, third, and fourth rows are the secondary, tertiary, and quaternary periods plotted separately; there are many fewer tertiary and quaternary periods. The period distribution of all four periods is still strongly peaked at <1 day.

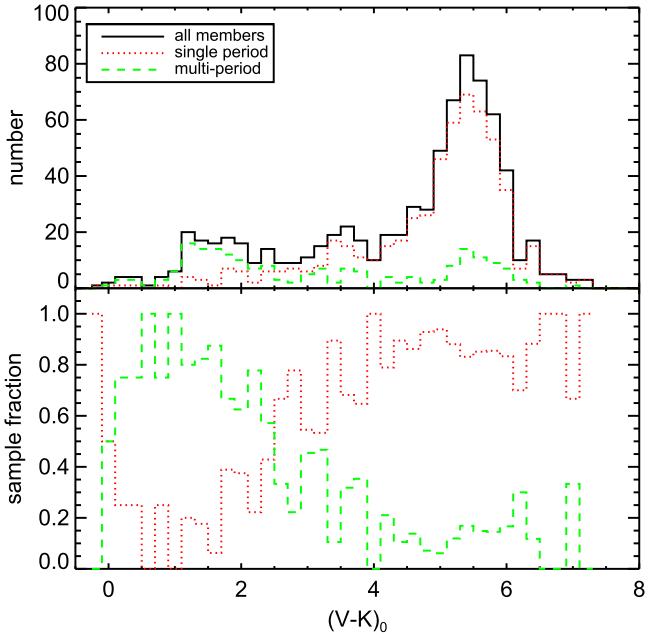

Figure 10. Distribution of $(V - K_s)_0$ for the ensemble, with the single (red dotted) and multiple (green dashed) populations called out. The top panel is absolute numbers, and the botttom is the sample fraction. The earlier types (bluer colors) are preferentially multiperiodic, and the later types (redder colors) are preferentially single-period, though about 30% of the earlier types have only one period that we can detect, and about 20% of the later types have multiple periods. Note that the place where the single-period and multiperiod distributions swap dominance in the lower panel is at about $(V - K_s)_0 \sim 2.6$, the location of the "kink" discussed in Paper III.

4. SINGLE-PERIOD AND MULTIPERIOD DISTRIBUTIONS

The broadest two categories of LC properties are simply single-period and multiperiod stars. This section looks at where the single-period and multiperiod stars fall in a variety of parameter spaces.

4.1. Period Distribution

Paper I discussed the overall period distribution. Because the sample of stars with one P dominates, the addition of all the secondary, tertiary, and quarternary periods does not change the distribution very much. Figure 9 separates the primary, secondary, tertiary, and quarternary periods found here. Even though there are far fewer tertiary and quarternary periods (10 with tertiary periods and 5 with quaternary periods), the distributions of all four periods are still strongly peaked at <1 day.

If all of the additional periods we determined are periods of secondary stars in unresolved binaries, then the "true" distribution of Pleiades rotation rates is the amalgamation of all the periods we determined, seen as the dotted line in Figure 9. However, it is unlikely that *all* of the additional periods are binaries; it is very likely that some are pulsation and many are differential rotation and/or spot evolution.

4.2. $(V - K_s)_0$ Colors

Figure 10 shows the distribution of $(V - K_s)_0$ values for the single-period and multiperiod categories. The earlier types (bluer colors, G and K dwarfs) are preferentially multiperiodic, and the later types (redder colors, M dwarfs) are preferentially single-period, though about 30% of the earlier types have only one period that we can detect, and about 20% of the later types have multiple periods. Many of the earlier types categorized as having only one period also have broad periodogram peaks, suggesting that they really are multiperiodic; we just cannot ascertain exactly what that additional frequency is.

The relationship found in Figure 10 could be explained by the ratio of active-region lifetime to rotation period. If the ratio is large, the LC is coherent even though it may have substructure. If the ratio is small, spots live for only a small number of rotations, giving rise to phase and amplitude modulation and peak splitting in the periodogram. If spots decay through diffusion and the diffusivity is related to the convective velocity, cooler stars will have longer-lived spots.

4.3. Amplitude Distribution

The LCs with multiple periods are on average slightly lower amplitude than those with single periods; see Figure 11 (and see Paper I, Section 3.3 for the definition of amplitude employed here). For the single-period sample, the mean amplitude (10%–90% of the points fall within this range, in magnitudes) is 0.0399 ± 0.0321 mag. For the multiperiod

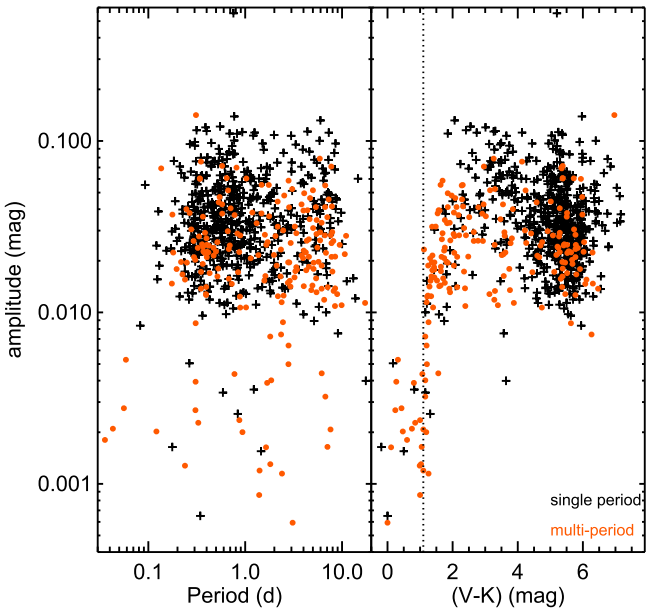

Figure 11. Amplitude (from the 10th to the 90th percentile), in magnitudes, of the periodic LCs, against P and $(V - K_s)_0$. The stars with single periods are black crosses, and those with multiple periods are orange circles. The vertical dotted line is at $(V - K_s)_0 = 1.1$ (see Paper III, where there is a linear version of this plot). Stars bluer than about $(V - K_s)_0 \sim 1.1$ have clearly lower amplitudes.

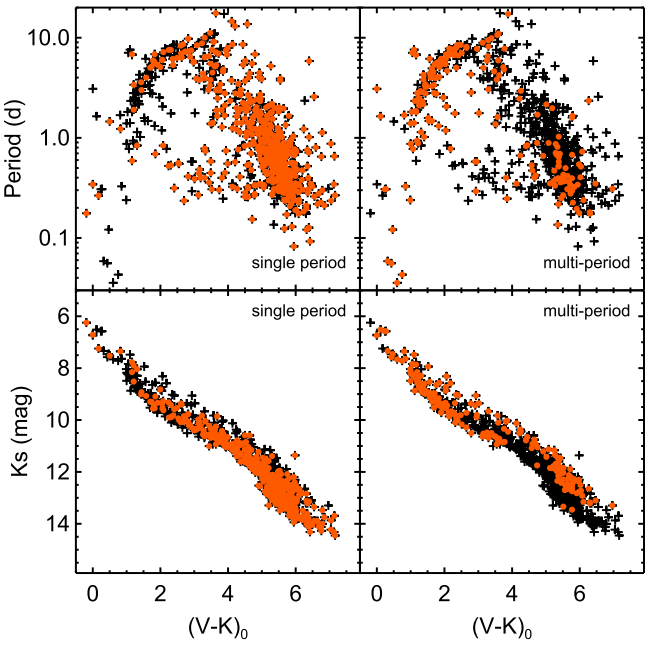

Figure 12. Plot of P vs. $(V - K_s)_0$ (top row) and K_s vs. $(V - K_s)_0$ (bottom row) highlighting the single-period (left) and multiperiod (right) populations. Most of the multiperiod stars are earlier-type stars, and the slow sequence is dominated by multiperiod stars. The fast sequence is dominated by single-period stars. Those stars in the fast sequence that are multiperiodic also tend to be the photometric binaries, suggesting that most of the M stars have single periods and may therefore be rotating as solid bodies.

sample, the mean is 0.0250 ± 0.0183 mag. Considering just $(V - K_s)_0 > 1.1$ to remove the possible and likely pulsators (also see discussion in Paper III), the single-period sample is nearly unchanged at 0.0403 ± 0.0321 mag and the multiperiod sample is 0.0274 ± 0.0176 mag; the multiperiod amplitudes are still on average smaller than the single-period amplitudes. Removing the distant resolved peaks as likely binaries (where the amplitude may be diluted by the companion) makes little difference in the means because there are relatively few of them. There are essentially no multiperiodic stars with amplitudes above 0.08 mag, but the stars with single frequencies include many up to 0.13 mag. This is likely why little if any of this diversity of multiperiod stars in the Pleiades has been discovered prior to these *K*2 data. (We note, however, two items of relevance: Stars with beating LCs have been observed in non-Pleiades CoRoT and *Kepler* data, such as Nagel et al. (2016). Magnitskii (2014) identified more than one period for 211025716/HII 296, interpreting it as substantial motions of spots in latitude and longitude; the *K*2 LC of this star(s) shows evidence of beating and has a complex periodogram peak, though we can only derive one period for it.)

The bias toward our finding single periods at later types is probably partially a selection effect (lower signal-to-noise ratio available in the fainter later types), but may also be due to different dynamo regimes or different spot latitude distributions. If the multiperiodic stars originate from spots at different latitudes (e.g., differential rotation), then the later types, which are largely rapidly rotating, either are rotating as solid bodies or primarily have high-latitude spots. We discuss this more below and in Paper III.

4.4. P *versus* $(V - K_s)_0$

Figure 12 shows the locations of the single and multiperiod stars in the P versus $(V - K_s)_0$ diagram and the color–magnitude diagram (CMD) for reference. As we suspected from Figure 10, it is primarily the earlier types that have multiple periods and the later types that have single periods. Most of the stars in the slowly rotating sequence with $1.1 \lesssim (V - K_s)_0 \lesssim 3.7$ have multiple periods. Most of the rest of the P versus $(V - K_s)_0$ diagram, particularly the M stars in the fast sequence (with $(V - K_s)_0 \gtrsim 5.0$), is composed of single-period stars. Interestingly, the M stars that are multiperiod in the fast sequence tend to also be above the main sequence, e.g., photometric binaries. For stars redder than $(V - K_s)_0 \sim 4$, nearly all the multiperiod LCs are also photometric binaries. Presumably, then, in those cases, the two periods we derive from the LC come from two different stars. Since most of the rest of the stars in the fast sequence seem to have single periods, and the two components of the photometric binary each have single periods, we suggest that most of the M stars have single periods and may therefore be rotating as solid bodies, or the timescale of any shift in latitude is much longer than the *K*2 campaign.

5. DISTRIBUTIONS OF CATEGORIES

While the prior section investigated where single- and multiperiod stars fall, we have many more than just two categories of LCs and periodogram structures; this section uses the full range of categories to explore the possible physical interpretations of the LC and periodogram shapes.

5.1. Beaters, Shape Changers, and Complex Peaks

We suggested above that beaters, shape changers, and complex peaks may all be different manifestations of more or less the same physics, that of latitudinal differential rotation and/or spot evolution. The beaters, shape changers, and complex

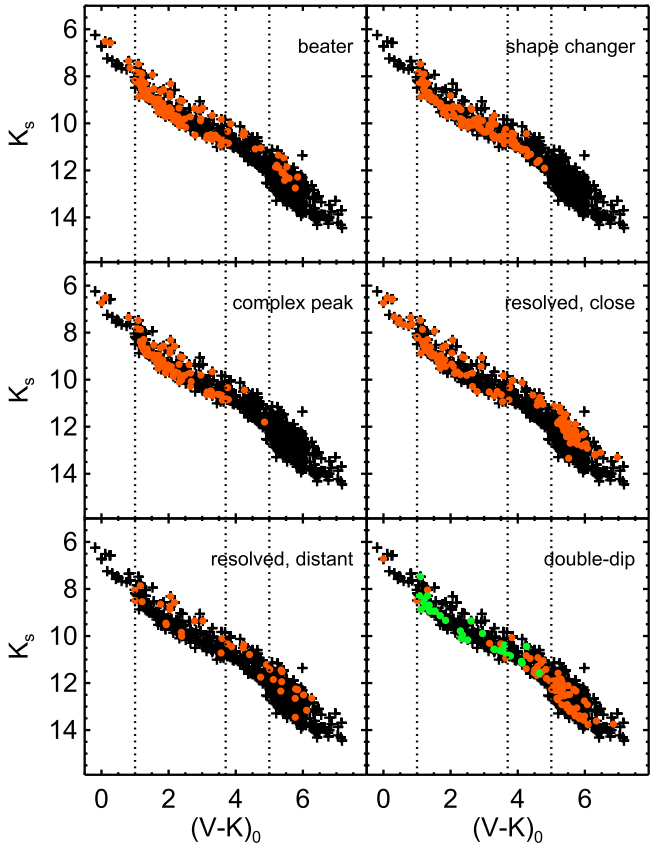

Figure 13. Plot of K_s vs. $(V - K_s)_0$, highlighting several of the LC categories described in the text. In each case, black crosses are the ensemble, and colored points highlight those objects of the category indicated. In the last panel, orange circles = stationary double-dip, and green circles = moving double-dip. The bluer stars (slow sequence) include most of the beaters, shape changers, and complex peaks and a significant number of the resolved close peaks. Resolved close peaks are also found in the redder stars (fast sequence), and these are largely the photometric binaries from Figure 12. Some beaters and resolved distant peaks are also photometric binaries. The double-dip LCs above are found throughout this diagram, but those showing movement within the campaign are distinctly higher mass. The dotted vertical lines are at $(V - K_s)_0 = 1.1$, 3.7, and 5.0, the divisions between the F stars (<1.1), slow sequence (1.1 to 3.7), the "disorganized region" (3.7 to 5.0), and the fast sequence (>5.0); see Papers I and III.

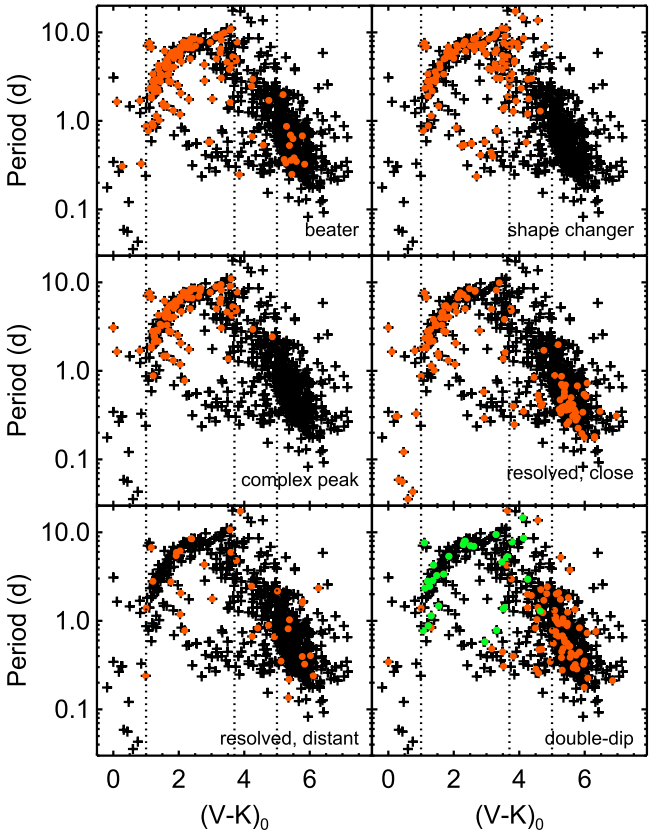

Figure 14. Plot of P vs. $(V - K_s)_0$, highlighting several of the LC categories described in the text. Notation (and the location of the dotted vertical lines) is the same as in Figure 13. The slow sequence consists of beaters, shape changers, complex peaks, and resolved close peaks. Resolved close peaks are also found in the fast sequence, and these are largely the photometric binaries from Figure 12. Some beaters and resolved distant peaks are also photometric binaries. The double-dip LCs above are found throughout this diagram, but those showing movement within the campaign are distinctly higher mass.

peaks are highlighted separately in the CMD in Figure 13 and the P versus $(V - K_s)_0$ diagram in Figure 14. All of these classes dominate the slow sequence at $1.1 \lesssim (V - K_s)_0 \lesssim 3.7$. The beaters make a larger excursion down into the fast-rotating sequence with $(V - K_s)_0 \gtrsim 5.0$ than the shape changer or complex peak classes, and the shape changers seem to dominate the "disorganized" region with $3.7 \lesssim (V - K_s)_0 \lesssim 5.0$. This is consistent with various manifestations of spot/spot group evolution and/or differential rotation. Especially for those shape changers (like Figure 2 or Figure 5) where one can see the spot evolution on timescales of the $K2$ campaign, the spot evolution is so slow, or the latitudinal differential rotation is so weak, that spots at different latitudes have very similar rotation rates; the $K2$ campaign is not long enough to distinguish that second frequency. If the "disorganized region" is a transition from strong differential rotation/fast spot evolution to solid-body rotation/a more stable spot or spot group, then this is consistent. Moreover, there seem to be two populations in the "disorganized region," fast and slow rotators; there is a gap near 1 day. The slower rotators are more likely to be shape changers than the fast rotators, again consistent with the faster rotators being solid-body rotators.

5.2. Double-dip LCs

On the whole, the double-dip LCs above are found throughout Figure 14 (for $(V - K_s)_0 > 1.1$), with no particular preference for color or rotation rate. This is consistent with our interpretation of them as spots on well-separated longitudes—the effect can occur whenever there are spotted stars, with no preference for color or rotation rate. However, those that show changing shapes over the $K2$ campaign (moving double-dip) are distinctly higher mass than those that show no shape changes (stationary double-dip). This is consistent with our proposed interpretation of spot evolution/migration over the $K2$ campaign for the moving double-dip. The lower-mass stars are more likely to be rotating as solid bodies, but spot lifetime also increases toward lower $T_{\rm eff}$.

5.3. Resolved Peaks

For the power spectra where we can resolve the specific periods in either close or distant pairs, there is probably more than one physical explantion underlying this observed property.

Figure 14 shows that the population with close peaks in the FGK stars seems also to track the slow sequence, again

consistent with differential rotation. However, in the fast sequence of M stars, there are also many more close peaks than the beater/shape changer/complex peak category. As can be seen in Figure 13, by the M stars, essentially all of the close resolved peaks are likely photometric binaries. This possibility is explored in more detail in Paper III.

The distant peaks seem to represent a more dispersed population in both Figures 13 and 14, less consistent with the large-scale structure in Figure 14. Both of these characteristics would be consistent with the distant peaks being more likely to be binaries as opposed to differential rotation or spot evolution. The population of late-type multiperiod photometric binaries from Figure 12 consists largely of the resolved close periods, though some beaters and resolved distant periods are also photometric binaries in this color range. For the distant peak stars, because the peaks are so widely spaced in period, forcing the peaks to be differential rotation would require an unphysically large shear. The most extreme case is 210930791/BPL 72, an M star, with two periods of ~19 and ~1.7 days; a more typical period difference for the resolved distant category is ~1.4 days.

6. ΔP DISTRIBUTIONS

As described in Section 3.4, for stars with at least two periods, we calculated a metric, $\Delta P/P_1$, which is the difference between the closest two periods in the periodogram, divided by the primary period. Figure 15 shows the relationship between this metric and period. The division between close and distant peaks at $\Delta P/P_1 = 0.45$ can be seen there; there are some stars with both close and distant peaks. Pulsators (the δ Scutis) are often outliers in this diagram. (The possible γ Dors, having periods comparable to the rotation periods, are not outliers in this diagram.)

The linear feature in the lower right of Figure 15 is composed of beaters and complex peaks, e.g., likely attributable to differential rotation (or spot/spot group evolution). Most shape changers and double-dip stars are single-period stars, so few of them can appear in this diagram, but those that do are found throughout this diagram. While there is scatter, most of the stars in the linear feature in the lower right of Figure 15 become the slow sequence in the P versus $(V - K_s)_0$ plot, and most of the multiperiod stars in the slow sequence in the P versus $(V - K_s)_0$ plot populate the linear feature in the lower right of Figure 15.

The concentration of sources near $P \sim 0.4$ and $\Delta P/P_1 \sim 0.3$ in Figure 15 largely populates the M star fast sequence in the P versus $(V - K_s)_0$ plot. These fast-rotating M stars are, as we have seen above, likely to be solid-body rotators. Thus, these stars for which we can derive a second period are likely to be binaries. They lie in a different portion of Figure 15 than the stars likely to be differentially rotating. For completeness, we note that a few of the fast-rotating K stars are also located in this $P \sim 0.4$ and $\Delta P/P_1 \sim 0.3$ clump.

The two most likely physical explanations for the $(V - K_s)_0 < 4$ stars with close, resolved peaks are (a) spots at two widely separated longitudes, with significant evolution in spot size and/or shape over the *K*2 campaign, or (b) two or more spots/spot groups at different latitudes for a star with significant latitudinal differential rotation. In the latter scenario, within this linear feature, the faster the rotation rate is, the closer the peaks are, suggesting weaker differential rotation in faster rotators—consistent with the fastest rotators (those that do not appear in this plot because they do not have multiple peaks) rotating as solid bodies.

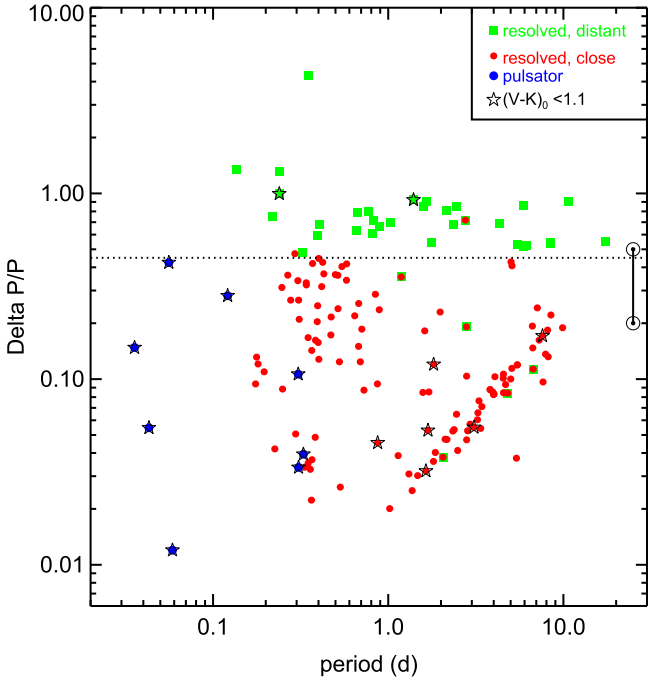

Figure 15. Plot of $\Delta P/P_1$ vs. P for pulsators (blue circles), resolved distant peaks (green squares), and resolved close peaks (red circles). An additional black star indicates that those stars have $(V - K_s)_0 \leqslant 1.1$ (see Paper III). The range of possible values for the Sun is included for reference ($\odot$); if one takes as ΔP the range of periods measured where sunspots occur, $\Delta P/P_1 \sim 0.1$–0.2, but if one takes the full range of ΔP, equator to pole, $\Delta P/P_1 \sim 0.5$. The dotted line is at $\Delta P/P_1 = 0.45$ and denotes the boundary between close and distant resolved peaks. Some objects are tagged as both close and distant peaks (e.g., there are at least three periods in these objects, two of which are close and a third of which is not close). Pulsators (δ Scutis) are largely outliers. The linear feature in the lower right predominantly becomes the slow sequence found in the P vs. $(V - K_s)_0$ plot. The clump of sources near $P \sim 0.4$ and $\Delta P/P_1 \sim 0.3$ becomes the M star fast sequence in the P vs. $(V - K_s)_0$ plot. The lack of sources below the linear feature is largely an observational bias.

The surface of the Sun rotates differentially, with a relative shear α (where $\alpha\Omega_{eq} = (\Omega_{eq} - \Omega_{pole})$) of 0.2; that is, the pole rotates 20% more slowly than the equator. If one assumes that the full range (pole to equator) could be measurable in these LCs, $\Delta P/P_1 \sim 0.5$; if one takes only the range over which sunspots are found, $\Delta P/P_1 \sim 0.2$. So, the Sun in Figure 15 lies more or less along the extension of the slowly rotating sequence of stars. Reinhold et al. (2013) have analyzed data from the original *Kepler* field for active low-mass stars and also find a good correlation between α and rotation period, though with much more scatter than we see in the Pleiades (their sample of field stars is much less homogeneous in age and metallicity than our sample).

Reinhold et al. argue that the sloping lower bound to the points in their figure is primarily an observational bias—they simply could not resolve two peaks in the LS periodogram if those two periods would place them below that lower bound. The lower bound to the linear feature in Figure 15 is probably also largely an observational bias for our data. We created a grid of synthetic models with known, noise-free, sinusoidal periods of comparable amplitude to test the limits of our approach to resolve the constituent periods. Under these conditions, it becomes harder to resolve periods below the linear feature. Recovery of the two periods is not precluded, but it becomes less likely, as the relative amplitudes and phasing of the constituent periods become more important.

However, no such detection bias exists immediately above the linear feature in our plot, from which we infer that for a coeval, young population there is a well-defined degree of differential rotation at a given mass, at least once the star is part of the slowly rotating sequence. (We note, however, that the role of spot/spot group evolution may also be important for interpretation of these LCs.)

Recently, Balona & Abedigamba (2016) found a similar relationship for differentially rotating stars in the main *Kepler* field. They find that $\Delta\Omega/\Omega$ as a function of Ω decreases sharply with rotation rate; transforming Figure 15 to that parameter space finds that our linear feature is consistent with their derived relationship.

7. CONCLUSIONS

We have continued our analysis of the *K*2 Pleiades light curves, finding complicated multiperiod behavior that we have grouped into categories. About 24% of the sample has multiple, real frequencies in the periodogram, sometimes manifesting as obvious beating in the LCs. These LCs can fall into categories of those having complex and/or structured periodogram peaks, unresolved multiple periods, and resolved multiple periods. These are likely due to latitudinal differential rotation and/or spot/spot group evolution. About 13% of the sample seems to have one period in the power spectrum, but the LC is seen to undergo substantial changes over the *K*2 campaign. These may be cases where the spot/spot group evolution is slow over the 72 day *K*2 campaign, or cases in which the latitudinal differential rotation is so weak that 72 days is not enough time to separate the nearly identical periods. About 1% of the objects in the sample are multiperiod because they are likely δ Scuti pulsators. About 12% of the objects in the the sample have double-dipped or (double-humped) LCs that redistribute power into peaks in the power spectrum other than the main period. These LCs are probably a result of spots on well-separated longitudes on the star. In six cases, the LCs have stable, shallow, angular patterns in the phased LC that affect a relatively small fraction of the phase coverage. These shallow flux dips may be due to transits or eclipses of orbiting clumps or clouds near the Keplerian corotation radius.

There are correlations of these broad categories with location in the P versus $(V-K_s)_0$ diagram. The slow sequence is dominated by complex and/or structured peaks, unresolved multiple periods, and resolved multiple periods; latitudinal differential rotation is likely to be happening in these higher-mass stars. The fast sequence is dominated by single-period stars; these are likely to be rotating as solid bodies. The transition between the fast and slow sequence is dominated by the shape-changing LCs. Multiperiod identifications among the lower-mass stars are likely to be binaries. Some multiperiod identifications among the higher-mass stars may be multiples or even pulsation, but the P we have chosen is the one we believe to be closest to the rotation period (that for the primary at least), so this ambiguity is unlikely to affect our results.

For those stars where we can detect at least two periods, we can calculate $\Delta P/P_1$, which is the difference between the closest two periods in the periodogram, divided by the primary period. In the plot of $\Delta P/P_1$ versus P_1, there is a striking linear feature in the lower right. It is composed of stars whose LCs are categorized as beaters and complex peaks, and they become the slow sequence in P versus $(V-K_s)_0$. While nondetection of periods below this linear feature is likely an observational bias, no such bias affects the distribution above the linear feature. Given that, there is a well-defined correlation between the degree of latitudinal differential rotation and period for our sample.

We continue discussion of these results in Paper III (Stauffer et al. 2016), which speculates about the origin and evolution of the period distribution in the Pleiades.

We thank R. Stern and T. David for helpful comments on draft manuscripts. A.C.C. acknowledges support from STFC grant ST/M001296/1.

Some of the data presented in this paper were obtained from the Mikulski Archive for Space Telescopes (MAST). Support for MAST for non-*HST* data is provided by the NASA Office of Space Science via grant NNX09AF08G and by other grants and contracts. This paper includes data collected by the *Kepler* mission. Funding for the *Kepler* mission is provided by the NASA Science Mission directorate.

This research has made use of the NASA/IPAC Infrared Science Archive (IRSA), which is operated by the Jet Propulsion Laboratory, California Institute of Technology, under contract with the National Aeronautics and Space Administration. This research has made use of NASA's Astrophysics Data System (ADS) Abstract Service and of the SIMBAD database, operated at CDS, Strasbourg, France. This research has made use of data products from the Two Micron All-Sky Survey (2MASS), which is a joint project of the University of Massachusetts and the Infrared Processing and Analysis Center, funded by the National Aeronautics and Space Administration and the National Science Foundation. The 2MASS data are served by the NASA/IPAC Infrared Science Archive, which is operated by the Jet Propulsion Laboratory, California Institute of Technology, under contract with the National Aeronautics and Space Administration. This publication makes use of data products from the *Wide-field Infrared Survey Explorer*, which is a joint project of the University of California, Los Angeles, and the Jet Propulsion Laboratory/California Institute of Technology, funded by the National Aeronautics and Space Administration.

Facilities: Kepler, *K*2, *Spitzer*, 2MASS.

REFERENCES

Balona, L., & Abedigamba, O. 2016, MNRAS, 461, 497
Balona, L., Catanzaro, G., Abedigamba, O., Ripepi, V., & Smalley, B. 2015, MNRAS, 448, 1378
Balona, L., Guzik, J., Uytterhoeven, K., et al. 2011, MNRAS, 415, 3531
Balona, L., Krisciunas, K., & Cousins, A. 1994, MNRAS, 290, 905
Bouy, H., Bertin, E., Sarro, L., et al. 2015, A&A, 577, 148
Boyajian, T., LaCourse, S., Rappaport, A., et al. 2016, MNRAS, 457, 3988
Bradley, P., Guzik, J., Miles, L., et al. 2015, AJ, 149, 68
Breger, M. 1972, ApJ, 176, 367
Breger, M. 1979, PASP, 91, 5
Collier Cameron, A. 1988, MNRAS, 233, 235
Collier Cameron, A., & Robinson, R. 1989, MNRAS, 236, 57
Covey, K., Agüeros, M., Law, N., et al. 2016, ApJ, 822, 81
Davenport, J., Herbb, L., & Hawley, S. 2015, ApJ, 806, 212
Fox Machado, L., Michel, R., Álvarez, M., Fu, J., & Zurita, C. 2011, RMxAX, 40, 237
Fox Machado, L., Pérez Hernández, F., Suárez, J., Michel, E., & Lebreton, Y. 2006, A&A, 446, 611
Gillen, E., Aigrain, S., McQuillan, A., et al. 2014, A&A, 562, A50
Gillen, E., Aigrain, S., Terquem, C., et al. 2016, A&A, submitted
Gray, R., Napier, M., & Winkler, L. 2001, AJ, 121, 2148
Hartman, J., Bakos, G., Kovács, G., & Noyes, R. 2010, MNRAS, 408, 475
Howell, S., et al. 2014, PASP, 126, 398
Kahraman Aliçavuş, F., Niemczura, E., et al. 2016, MNRAS, 458, 2307
Karoff, C., Metcalfe, T., Chaplin, W., et al. 2009, MNRAS, 399, 914
Kaye, A., Handler, G., Krisciunas, K., Poretti, E., & Zerbi, F. 1999, PASP, 111, 840

Krisciunas, K. 1994, ComAp, 17, 213
Magnitskii, A. 2014, AstL, 40, 628
McQuillen, A., Aigrain, S., & Mazeh, T. 2013, MNRAS, 432, 1203
Melis, C., Reid, M., Mioduszewski, A., Stauffer, J., & Bower, G. 2014, Sci, 345, 1029
Mendoza, E. 1956, ApJ, 123, 54
Metcalfe, T., Creevey, O., & Christensen-Dalsgaard, J. 2009, ApJ, 699, 373
Morin, J., Donati, J.-F., Petit, P., et al. 2008, MNRAS, 390, 567
Morin, J., Donati, J.-F., Petit, P., et al. 2010, MNRAS, 407, 2269
Nagel, E., Czesla, S., & Schmitt, J. H. M. M. 2016, A&A, in press (arXiv:1603.06502)
Oppenheimer, B., Basri, G., Nakajima, T., & Kulkarni, S. 1997, AJ, 113, 296
Rebull, L., Stauffer, J., & Cody, A. 2016, AJ, 152, 113 (Paper I)
Reinhold, T., Reiners, A., & Basri, G. 2013, A&A, 560, A4
Russell, H. N. 1906, ApJ, 24, 1
Scargle, J. D. 1982, ApJ, 263, 835
Sierchio, J., Rieke, G., Su, K., et al. 2010, ApJ, 712, 1421
Stauffer, J., Rebull, L., Bouvier, J., et al. 2016, AJ, 152, 115 (Paper III)
Stauffer, J., Schultz, G., & Kirkpatrick, J. D. 1998, ApJ, 499, 199
Terquem, C., Sorensen-Clark, P., & Bouvier, J. 2015, MNRAS, 454, 3472
Vanderburg, A., Johnson, J., & Rappaport, S. 2015, Natur, 526, 546
Xiong, D., Deng, L., Zhang, C., & Wang, K. 2016, MNRAS, 457, 3163